Performance of an internally cooled and heated desiccant-coated heat and mass exchanger
Effectiveness criteria and design methodology

Jagirdar, Mrinal; Lee, Poh Seng; Padding, Johan T.

DOI
10.1016/j.applthermaleng.2021.116593

Publication date
2021

Document Version
Accepted author manuscript

Published in
Applied Thermal Engineering

Performance of an internally cooled and heated desiccant-coated heat and mass exchanger: effectiveness criteria and design methodology

Mrinal Jagirdar[a,*], Poh Seng Lee[b], Johan T. Padding[c]

[a]*Multi-Disciplinary Laboratory, National University of Singapore, Singapore 117581*
[b]*Department of Mechanical Engineering, National University of Singapore, Singapore 117575*
[c]*Process & Energy department, Delft University of Technology, The Netherlands*

Abstract

Internally cooled and heated desiccant-coated heat and mass exchangers (ICHDHMX) driven by low-grade heat are very attractive owing to their energy-saving potential, especially for applications where substantial moisture removal (such as air-conditioning) is a necessity. In this paper, we derive equations for the performance of an ideal ICHDHMX, allowing us to define humidity-ratio effectiveness (ε_Y) and relative-humidity effectiveness (ε_{RH}) such that their values approach 1 as the performance approaches that of an ideal ICHDHMX. Besides an equation-based approach, an easy-to-use psychrometric-chart based approach is presented to determine the performance of an ideal ICHDHMX. We invoke conservation principles to ascertain whether or not it is feasible to use the ICHDHMX for a given set of inlet conditions of air and water streams for dehumidification and regeneration. The dimensions of the ICHDHMX can be determined using this methodology, not even requiring knowledge of a tuning parameter unless a precise outlet specific humidity is required. Simulations are conducted for cases involving three incoming hot water temperatures (38, 44 and 50°C) and several mixing ratios of room return air (25°C at 0.011 kg/kg dry air) and outdoor air (32°C at 0.02 kg/kg dry air), typical of warm and humid weather conditions. For all cases, the cool-water inlet is fixed at 30°C. The results show that even when the dehumidification air-stream humidity is high, if the regeneration air-stream humidity is low (typical of room-exhaust air), the operation of an ICHDHMX is feasible using a low regeneration temperature of only 38°C. When the regeneration temperature is 50°C, the exchanger can operate under the complete range of humidity conditions tested. A cooling coefficient of performance up to 9.8 and effectiveness value up to 0.88 is realized, while the fluid power required is generally very low. These findings substantiate the case for commercial adoption of this technology for air-conditioning.

Keywords: desiccant dehumidification; air conditioning; HVAC; desiccant coated heat exchanger; modeling; fin tube heat exchanger

1. Introduction

Heating, ventilation and air conditioning (HVAC) typically accounts for nearly 50% of the total energy consumption of a building and approximately 10–20% of the total energy consumption in advanced nations [1]. In addition to being responsible for enormous carbon emissions, conventional air-conditioning technologies also contribute exceedingly to the use of refrigerants that have a high global warming potential. As governments across the world become increasingly conscious about climate-change and as countries commit to reduce carbon emissions as well as the usage of refrigerants (Kigali Amendment), alternative air-conditioning technologies that promise high energy efficiency and reduced usage of refrigerants become attractive. To this end, researchers have proposed component as well as system level solutions to make air-conditioning technologies greener.

Desiccant assisted dehumidification technologies have been identified to be among the most promising technologies [2], especially in the tropical climate which is warm and humid, where the latent heat load can exceed the sensible load (for the fresh-air part). Conventional dehumidifiers such as desiccant wheels [3] dehumidify air adiabatically. This results in a substantial increase in the temperature of the dehumidified air. The adiabatic process also necessitates a much larger regeneration temperature (typically >80°C) for regeneration [4]. While there are a some researchers, such as Pandelidis et al.[5], who studied desiccant wheels under the availability of heat at moderate temperatures of 50 to 60°C, the assumed ambient air humidity was moderate (10-13 g/kg dry air). The use of desiccant wheels, especially for medium to high humidity environments, is hence restricted to places with availability of heat at medium to high temperature. To circumvent this difficulty with desiccant wheels, researchers [6–22] have focused their attention to internally cooled and heated (solid/liquid) desiccant systems, which facilitate quasi-isothermal dehumidification or simultaneous dehumidification and cooling. The water (or refrigerant) takes up the sorption heat during dehumidification, while it supplies the desorption heat during regeneration. The main advantage of this technology is that dehumidification is much more efficient and the required regeneration temperature is significantly lower than that required by desiccant wheels.

Most work on quasi-isothermal dehumidifiers has been experimental, as reviewed by Vivekh et al. [23]. Oh et al. [24] compared the performance of an adsorbent coated heat exchanger with a conventional granular adsorbent packed heat exchanger (widely used for adsorption chillers and desalination plants). They observed that although the amount of adsorbent used in the former was five times less, its adsorption capacity was two times that of the latter. Narayanan et al. [25] conducted a study on non-adiabatic (as opposed to conventional adiabatic) desiccant wheels containing an internal heat transfer structure with alternative channels for dehumidification and for indirect cooling of the dehumidification process. They concluded that the non-adiabatic desiccant wheel can increase dehumidification levels by 45-53% under otherwise identical supply air and regeneration air conditions. Sun et al. [26] compared the performance of a desiccant coated microchannel exchanger and desiccant coated fin-and-tube heat exchanger. They found that although the mass transfer coefficient of the former was 15% better than the latter, the pressure drop per unit area was 125% higher in the case of the former. Jagirdar et al. [27] retrofitted desiccant coated fin-tube heat exchangers in the upstream part of the air handling unit (AHU) of a conventional air-conditioning system. For the case of 100% fresh-air intake, the retrofitted units managed 39% of the total cooling load while only utilizing low-grade heat from the condenser unit.

While a number of researchers have developed models for simulation of desiccant wheels, as reviewed by Ge et al. [28], there are few who have developed first-principles based models for solid-desiccant based quasi-isothermal dehumidifiers. Simulations were carried out by Ge et al. [29] for a cross-flow desiccant coated heat exchanger using a one-dimensional mathematical model. A model was developed by Jeong et al. [30] to simulate a fixed desiccant bed that is cooled by water (flowing perpendicularly to the air-flow) during dehumidification. Jagirdar and Lee [18] developed a 2-D model for simulation of a desiccant-coated fin tube heat exchanger that takes into account the difference between tube and fin temperature as well as the solid-side mass transfer resistance. Zhou et al. [19] developed a model to simulate an internally cooled desiccant wheel. Hua et al. [31] developed a model to simulate a solid-desiccant based heat pump. Despite the sophistication of some of these models, they have not been used to test the limiting thermodynamic performance.

In this work we will analyse the ideal thermodynamic performance of a desiccant system in the specific configuration of an internally cooled and heated desiccant-coated heat and mass exchanger (ICHDHMX). The ideal performance is then used as a reference in formulation of a performance indicator. Many researchers [32–38] use specific-humidity effectiveness and relative humidity effectiveness as performance indicators, but these pertain to an adiabatic dehumidification process. Despite recent advances in the field of internally cooled/heated (non-adiabatic) desiccant dehumidifiers, a proper definition of humidity-ratio effectiveness (ε_Y) and relative humidity effectiveness (ε_{RH}), based on validated ideal performance is missing. Knowledge regarding the performance of an ideal desiccant dehumidification system and a simple procedure (such as a psychrometric-chart based method) will be useful in determining the viability of such systems and to gauge their limiting performance, as illustrated by Collier [39] as well as Nobrega and Brum [36] for adiabatic desiccant wheels. Here we will extend the analysis to a non-adiabatic ICHDHMX system (henceforth simply referred to as the heat and mass exchanger, HMX).

This paper is organised as follows. In section 2, we present a two-dimensional heat and mass transfer model of the HMX, which is an altered version of our previous model [18]. In section 3, the concept of an ideal HMX is presented, with a discussion regarding its characteristics. Using the ideal performance as a reference, a novel definition of humidity-ratio effectiveness (ε_Y) and relative-humidity effectiveness (ε_{RH}) is presented, such that it is analogous to the definition of heat transfer effectiveness of heat exchangers. Additionally, a new and simple psychrometric-chart based methodology is developed for the same purpose. Based on this, in section 4, a novel yet simple feasibility check and design methodology is developed (avoiding complicated numerical modelling), which not only helps ascertain the feasibility of a HMX (given the inlet conditions of air and water streams during dehumidification and regeneration) but also helps determine the critical geometrical parameters of the HMX in a straight-forward manner without resorting to the complex task of comprehensive modelling and simulation work. In section 5, experimental results in the literature are used to validate the two-dimensional heat and mass transfer model. The ideal performance of the HMX (from section 3) is confirmed by conducting simulations of the two-dimensional model at close-to-ideal conditions. Several cases are then studied which pertain to the retrofitting of HMXs to existing conventional vapour-compression based air-conditioning system, which shows the viability for commercial adoption of this technology for air-conditioning. We end with our conclusions in section 6 and recommendations for future work in section 7.

Nomenclature

A	area (m^2)
C	capacitance rate (W/K)
C_f	correction factor
C_p	specific heat (J/(kg·K))
C_r^*	total matrix heat capacity ratio
d	diameter (m)
D	mass diffusivity (m^2/s)
De	dehumidification moisture removal (kg/kg d.a.)
E	specific enthalpy (J/(kg·K))
f_d	sorbent mass fraction
h	heat transfer coefficient (W/(m^2·K))
H_d	thickness of the desiccant layer (m)

H_f	fin thickness (m)
h_m	mass transfer coefficient (m/s)
I_0	modified zero-order Bessel function of the first kind
I_1	modified first-order Bessel function of the first kind
K_0	modified zero-order Bessel function of the second kind
K_1	modified first-order Bessel function of the second kind
k_d	desiccant thermal conductivity (W/(m·K))
k_f	fin thermal conductivity (W/(m·K))
L_x	fin length (air-flow direction) (m)
L_y	fin width (m)
L_z	tube length (along the height of the HMX) (m)
m, M	mass (kg)
$\dot{m}$	mass flow rate (kg/s)
N_t	total number of tubes
P_f	fin pitch (m)
Q	volume flow rate (m^3/s)
q	rate of heat transfer (W)
q''_{gen}	rate of heat flux (W/m^2)
q_{ads}	adsorption heat (J/kg)
$r_{1,i}$	tube inner radius (m)
$r_{1,o}$	tube outer radius (m)
r_2	outer radius of the equivalent annular fin (m)
T	temperature (°C)
t	time (s)
t_1	dehumidification process time-period (s)
t_2	regeneration process time-period (s)
U	velocity (m/s)
W	sorbate uptake
X_l	tube-pitch along the longitudinal direction (m)
X_t	tube-pitch along the transverse direction (m)
Y	specific humidity (kg moisture/kg dry air)
ΔP	pressure drop (Pa)
β	factor accounting for relatively smaller tube area near the fin-ends
ε_d	desiccant porosity
ε_{RH}	relative-humidity effectiveness
ε_T	heat-transfer effectiveness
ε_Y	specific-humidity effectiveness
$\eta_{f,app}$	apparent fin efficiency
θ	non-dimensional temperature
ρ	density (kg/m^3)
υ_r	pore radius of the desiccant (m)
ϕ	relative humidity

Sub/ Super-scripts

0	initial value ($t = 0$)
a	air
app	apparent
atm	atmospheric
avg	time-averaged value
cw	concentration wave
d	desiccant
de	dehumidification
dry	dry portion of air
eq	equivalent
f	fin
i	inner
in	inlet
min	minimum
max	maximum
m_{eq}	matrix equivalent
o	outer/out
r	room

re	regeneration
s	surface
s-avg	spatial average
t	tube
tw	thermal wave
v	vapour
w	water
*	limiting value
‾	length of the line-segment
Abbreviations	
CL	cooling load handled
COP	coefficient of performance
FP	fluid power (delivered by blowers and pumps)
HMX	heat and mass exchanger
ICHD-HMX	internally cooled and heated desiccant-coated heat and mass exchanger

2. Heat and mass transfer model

2.1. Hybrid air-conditioning system

The hybrid air-conditioning system, consisting of an HMX and a conventional (vapor-compression refrigeration) HVAC system with a water-cooled condenser, is shown in Figure 1. Two HMX units operate simultaneously. While one unit dehumidifies the air-stream to be supplied to the room, the other unit undergoes regeneration using a second air-stream; the two units are periodically switched between dehumidification and regeneration. The HMX dehumidifying air is supplied with cool water from the auxiliary condenser or the cooling tower. The HMX getting regenerated is supplied with hot water, either from the water-cooled condenser or a low-grade solar/waste heat source. The two HMX units switch their operations periodically to achieve continuous dehumidification of the working air with the help of valves and dampers that control water-flow and air-flow, respectively. The dehumidified air passes through the air handling unit (AHU) where it gets cooled. Depending on the application, either the room-return air or fresh air or a mixture of the two may be utilized as the regeneration air-stream.

The heat and mass transfer model for the HMX is similar to that in Jagirdar and Lee [18]. Modifications of the model made in this work are as follows. (i) The 'equivalent annulus method' is used to estimate fin-efficiency (this linearizes the equations pertaining to energy-conservation). (ii) The thermal mass of water within the tubes is incorporated in the governing equations. A very concise form of the governing equations is presented here; for details we refer to the Supplementary Material. Equations defining properties of the desiccant, heat and mass transfer coefficients as well as the pressure drop relations for the air and water streams are also presented therein. We refer to Jagirdar and Lee [18] for a detailed explanation of the computational grid and other simulation details.

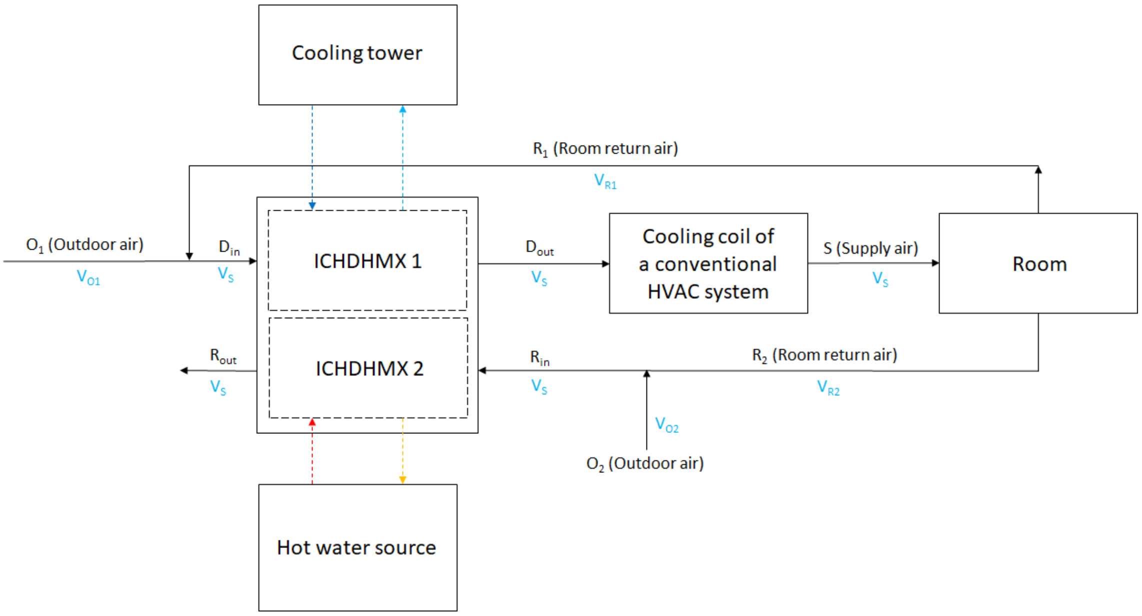

Figure 1: Schematic of a hybrid air-conditioning system consisting of a conventional central air-conditioning system augmented with ICHDHMX. Note that the air-stream labels are consistent with those in Table 5

2.2. Governing equations

Figure 2 shows a schematic picture of the fin tube heat exchanger geometry and the coordinate system used in our work. Fins are installed perpendicular to the tubes carrying the water and used to enhance the heat and mass transfer from the air flowing parallel to the fins. Note that we approximate the fin tube heat exchanger as a 2D geometry. This is justified because ideally no change in fluid flow, heat and mass transfer phenomena is expected along the transverse direction (along the y-axis) owing to the repeating structure of the geometry.

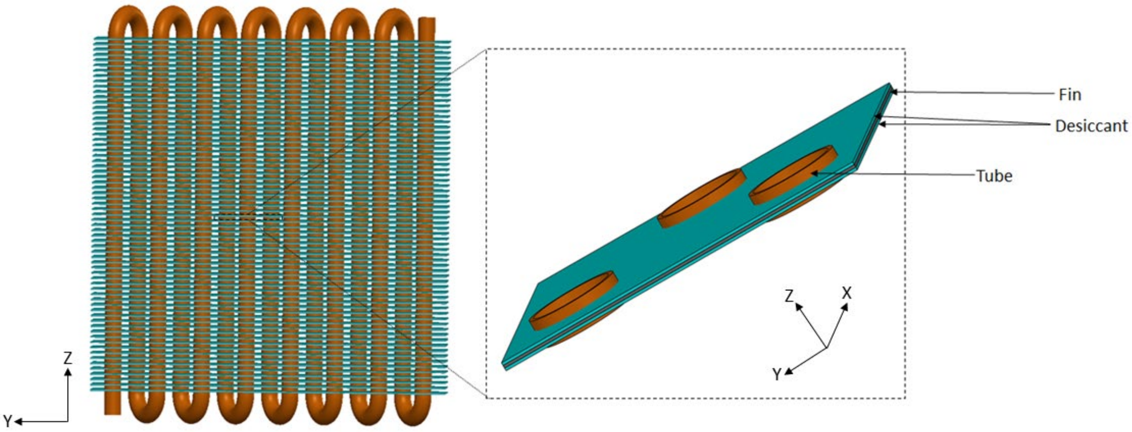

Figure 2: A fin-tube heat exchanger which is coated with a desiccant (internally cooled and heated desiccant-coated heat and mass exchanger)

The governing equations describing mass and heat transfer are given below. Model assumptions, boundary conditions and correlations for the transport coefficients are given in the Supplementary Material. Equations (1) and (2) ensure moisture mass conservation in the air-channel and the desiccant domain, respectively, while equations (3) and (4) ensure energy conservation in the air-channel and desiccant domain. Equation (5) relates the tubes temperature with that of the air and desiccant; the factor κ is derived in equation (12). Energy conservation in the water-stream is ensured by equation (6). Coefficient values of the aforementioned equations are given by Equation (7).

$$\frac{\partial Y_a}{\partial t}+U_a\frac{\partial Y_a}{\partial x}=\psi_1(Y_{d,s}-Y_a) \tag{1}$$

$$\frac{\partial Y_d}{\partial t}=D_{d,a}\left(\frac{\partial^2 Y_d}{\partial x^2}+\frac{\partial^2 Y_d}{\partial z^2}\right)+\psi_2 \tag{2}$$

$$\frac{\partial T_a}{\partial t}+U_a\frac{\partial T_a}{\partial x}=\psi_3(T_d-T_a)+\psi_3' \tag{3}$$

$$\psi_4\frac{\partial T_d}{\partial t}+\psi_5\frac{\partial T_a}{\partial t}=\psi_6 T_d+\psi_7 T_a+\psi_8 \tag{4}$$

$$T_t=T_a+\frac{q''_{gen}}{h_a}+\kappa h_a\left(T_d-T_a\right)-\kappa q''_{gen} \tag{5}$$

$$T_{w,s-avg}=\frac{2T_{w,in}+\psi_9 T_{t,s-avg}+\psi_{10}T^0_{w,s-avg}}{2+\psi_9+\psi_{10}} \tag{6}$$

The coefficients are evaluated as follows.

$$\psi_1=\frac{2h_m}{H_a}\ ;\ \psi_2=\frac{-(1-\varepsilon_d)\rho_d f_d}{\varepsilon_d\rho_{a,dry}}\left(\frac{\partial W}{\partial t}-D_s\left(\frac{\partial^2 W}{\partial x^2}+\frac{\partial^2 W}{\partial z^2}\right)\right);$$

$$\psi_3=\frac{2h_a}{H_a\rho_a C_{p,a}}+\frac{2h_m C_{p,v}}{H_a C_{p,a}}(Y_{d,s}-Y_a)+\frac{h_a^2\pi r_{1,o}\kappa}{\beta\rho_a C_{p,a}A_d};\psi_3'=\frac{h_a\pi r_{1,o}q''_{gen}}{\beta\rho_a C_{p,a}A_d}\left(\frac{1}{h_a}-\kappa\right)$$

$$\psi_4=\left(\rho C_p\right)_{m_{eq}}A_d\left(\frac{H_f}{2}+H_d\right)+\frac{m_t C_{p,t}\kappa h_a}{\beta}\ ;\ \psi_5=\frac{m_t C_{p,t}}{\beta}\left(1-\kappa h_a\right);\psi_6=-\left(h_a A_d+\frac{\kappa h_a^2 A_{t,a}}{\beta}+\frac{h_w A_w \kappa h_a}{\beta}\right);$$

$$\psi_7 = \left(h_a A_d + \frac{\kappa h_a^2 A_{t,a}}{\beta} - \frac{h_w A_w}{\beta}\left(1-\kappa h_a\right) \right);$$

$$\psi_8 = q''_{gen}\left(A_d - \left(\frac{1}{h_a}-\kappa\right)\left(\frac{h_a A_{t,a}}{\beta}+\frac{h_w A_w}{\beta}\right)\right) + \frac{h_w A_w T_{w,s-avg}}{\beta} - \frac{m_t C_{p,t}}{\beta}\left(\frac{1}{h_a}-\kappa\right)\frac{\partial q''_{gen}}{\partial t};$$

$$\psi_9 = \left(\frac{h_w A_{t,i,total}}{\dot{m}_w C_{p,w}} \right); \psi_{10} = \frac{\rho_w \pi d_{1,i}^2 N_t L_z}{4 \dot{m}_w \,\delta t} \tag{7}$$

2.3. Tube temperature and the apparent fin-efficiency

The periodic segment of the fin around each tube is an irregular polygon (refer to the Supplementary material for more details). Therefore, the fin-efficiency is approximated by the equivalent-annulus method [40]. The outer radius of the equivalent fin is obtained in equation (8) by equating the wetted area of the equivalent annular fin with that of the actual polygonal fin.

$$r_2 = \frac{1}{2}\sqrt{\frac{4}{\pi} X_l X_t} \tag{8}$$

For an annular fin with heat generation, the fin efficiency is given by equation (9) (for a derivation, see [18])

$$\eta_{f,app} = \frac{r_1\sqrt{2h_a k_f H_f}\left(T_t - T_a - \frac{q''_{gen}}{h_a}\right)\left(\frac{K_1(mr_1)I_1(mr_2)-I_1(mr_1)K_1(mr_2)}{K_0(mr_1)I_1(mr_2)+I_0(mr_1)K_1(mr_2)}\right)+(r_2^2-r_1^2)q''_{gen}}{h_a(r_2^2-r_1^2)(T_t-T_a)} \tag{9}$$

where

$$q''_{gen} = \frac{q_{ads}(1-\varepsilon_d)\rho_d f_d W_{eq}}{A_d}\int\limits_{u.c.}\int\left(\frac{\partial W}{\partial t} - D_s\left(\frac{\partial^2 W}{\partial x^2}+\frac{\partial^2 W}{\partial z^2}\right)\right)\delta z\,\delta x \tag{10}$$

Equating the definition of fin-efficiency ($\eta_{f,app}$ = $(T_d-T_a)/(T_t-T_a)$) with equation (9) and re-arranging terms yields equation (11).

$$T_t = T_a + \frac{q''_{gen}}{h_a} + \kappa\left(h_a\left(T_d - T_a\right) - q''_{gen}\right) \tag{11}$$

Here

$$\kappa = \frac{(r_2^2-r_1^2)}{r_1\sqrt{2h_a k_f H_f}}\left(\frac{K_0(mr_1)I_1(mr_2)+I_0(mr_1)K_1(mr_2)}{K_1(mr_1)I_1(mr_2)-I_1(mr_1)K_1(mr_2)}\right) \tag{12}$$

2.4. Cooling load, fluid power and coefficient of performance

The cooling-load that the HMX handles can be evaluated using equation (13), while that handled by the complete hybrid system (the HMX and the cooling-coil) is given by equation (14).

$$CL_{HMX} = \dot{m}_a(E_{HMX,in} - E_{HMX,o}) \tag{13}$$

$$CL_{total} = \dot{m}_a(E_{HMX,in} - E_{r,in}) \tag{14}$$

Enthalpies are evaluated by equation (15) for various air-states (temperature and specific humidity) using standard values for the specific heat of dry air and moisture within the air.

$$E = 10^3(1.006T + Y(2501 + 1.86T)) \tag{15}$$

The fluid power that pumps and blowers deliver to the water-streams and the air-streams of the two HMXs shown in Figure 1 is given by equation (16).

$$FP = (\Delta P_{a,de}Q_{a,de}) + (\Delta P_{a,re}Q_{a,re}) + (\Delta P_{w,de}Q_{w,de}) + (\Delta P_{w,re}Q_{w,re}) \tag{16}$$

Based on the compressor power-consumption, the coefficient of performance (COP) of the conventional vapor-compression refrigeration system $COP_{conventional}$ is taken as 4 [41,42], while for the hybrid system the COP_{hybrid} is evaluated using equation (17). Note here that the denominator is the compressor-work input after installation of the HMXs into the system assuming that the compressor COP remains constant (irrespective of the cooling load). Therefore, this is the (apparent) compressor COP after the system becomes a hybrid system.

$$COP_{hybrid} = \frac{CL_{total}}{\left(CL_{total} - CL_{HMX}\right)/COP_{conventional}} \tag{17}$$

3. Concept of an ideal HMX and definitions of effectiveness

3.1. *Introduction*

Effectiveness is an indispensable parameter that gauges the performance of heat/mass exchangers against the performance of an ideal heat/mass exchanger. In other words, effectiveness is a yardstick used to measure the degree of perfection of actual exchanger performance [40]. The heat-transfer effectiveness of a heat exchanger (ε_T) is defined as the ratio of heat transferred between two fluids flowing through that heat exchanger and the heat transferred (thermodynamically permissible maximum) between the same two fluids flowing through an ideal counter flow heat exchanger for the same inlet temperature and flow rates of the heat exchange fluids [43]; in an analogous manner, ε_Y of an internally cooled/heated desiccant-coated heat and mass exchanger may be defined as the ratio of the mass of moisture transferred between two fluids flowing through that exchanger and the mass transferred between the same two fluids flowing through an ideal exchanger, given the inlet temperature, humidity-ratio (specific humidity) and the flow-rates of the mass exchanging air/gas streams as well as the temperature of cool and hot water streams. Also, ε_{RH} of an internally cooled/heated mass regenerator may similarly be defined as the ratio of the difference between (apparent) inlet and outlet relative humidity (ϕ) of the air-stream and the maximum possible difference (that would occur in an ideal HMX) in ϕ of the air-stream. ε_Y is thus given by equation (18) while ε_{RH} is given by equation (19). Note that the form of equations (18) and (19) is similar to those used for desiccant wheels (see [32,37] for the equation defining ε_Y and [34,44] for the equation defining ε_{RH}).

$$\varepsilon_Y = \frac{M_{actual}}{M_{\max}} \tag{18}$$

$$\varepsilon_{RH} = \frac{\Delta\phi_{actual}}{\Delta\phi_{max}} = \frac{\phi^*_{a,in,de} - \phi_{a,o,de}}{\phi^*_{a,in,de} - \phi_{a,o,de,min}} \tag{19}$$

3.2. *Assumptions*

Due to the complexity of coupled heat and mass transport phenomena some assumptions are made to avoid undue mathematical complexity while ensuring the usefulness of the derived formula for humidity-ratio as well as relative humidity effectiveness.

(i) The sorption isotherm of the desiccant is only a function of relative humidity (i.e. not explicitly dependent on temperature). Desiccants having such sorption isotherms are predominant in the literature (see [23,28,31,34,39,44]).

(ii) Hysteresis in the desiccant adsorption/desorption isotherm is negligible.

(iii) The mass flow-rate of water-streams (cool as well as hot) is assumed to be very large (implying that these function as constant-temperature heat-sink and heat-source) so that there is negligible change between the inlet and outlet temperature of water. Note that in reality also the mass flow rate of water and its thermal capacitance are high. Therefore, the change in water temperature from inlet to outlet is expected to be relatively small, justifying the assumption for a limiting case.

3.3. Ideal HMX

3.3.1. Characteristics

Before characterizing an ideal HMX, it is important to note that from the point of view of mass-transfer, such exchangers are regenerators, while from the point of view of heat-transfer, they are primarily recuperators and to a small degree they are inadvertently regenerators (due to the non-zero thermal mass of the dehumidifier structure). An ideal exchanger would have the following characteristics:

1. The air-side (dehumidification and regeneration air-streams) heat and mass transfer resistance is negligible (product of air-side heat transfer coefficient and surface area is infinite).
2. The hot/cool water-side heat transfer resistance is negligible (product of water-side heat transfer coefficient and surface area is infinite).
3. The solid-side (fin and tube) heat-transfer resistance is negligible (a fin-efficiency of unity and infinite thermal conductivity).
4. Negligible mass transfer resistance as well as negligible diffusion time in the desiccant (high mass-transfer diffusivity and small thickness).

5. Negligible thermal mass of the system (solid structures and the water content within the tubes) so that C_r^* (total matrix heat capacity rate ratio) is negligible. Note that for exchangers that are meant to be used as a heat-regenerators, it is desirable that C_r^* be as high as possible from the perspective of heat transfer (see Shah and Sekulic [40]); for the present case, however, it is not desirable that the relatively hot regeneration air-stream and water-stream transfer heat to the cooler dehumidification air-stream and water-stream. Thus C_r^* must be minimized.
6. Switching between dehumidification and regeneration takes negligible time, so there is negligible carry-over/leakage between the streams (implying fast acting valves and dampers).
7. The ratio of total sorbate uptake capacity rate of the desiccant mass in the exchanger to the mass flow rate of air (the mass-transfer equivalent of C_r^*) is high (which implies that enough desiccant is available for adsorption/desorption throughout the process time-period so that it does not become saturated/dry).
8. The mass flow rate of water is infinite, so the temperature rise (drop) during dehumidification (regeneration) from the inlet (outlet) is negligible, ensuring minimum (maximum) temperature throughout the complete exchanger domain, thus maximizing (minimizing) the prevalent relative humidity in the domain for maximum adsorption (desorption).

3.3.2. Limiting performance

To ensure maximum moisture exchange between the two air-streams (as would be the case in an ideal HMX), the swing in the relative-humidity must be the maximum. The maximum relative humidity (see equation (20)) achievable during dehumidification corresponds to the minimum temperature (inlet cool-water temperature) of the cooling media and the maximum specific humidity (inlet humidity of air to be dehumidified). The minimum relative humidity (see equation (21)) achievable during regeneration corresponds to the maximum temperature (inlet hot-water temperature) of the heating media and the minimum specific humidity (inlet specific humidity) of regeneration air.

$$\phi^*_{a,in,de} = \phi(T_{w,in,de}, Y_{a,in,de}) \tag{20}$$

$$\phi^*_{a,in,re} = \phi(T_{w,in,re}, Y_{a,in,re}) \tag{21}$$

The minimum achievable humidity-ratio of dehumidified air (at the outlet) corresponds to the minimum value of relative humidity $\phi^*_{a,in,re}$ (equation (21)) achieved during regeneration and minimum temperature ($T_{w,in,de}$) achieved during dehumidification. The maximum achievable humidity-ratio of humidified air (at the outlet during regeneration) corresponds to the maximum value of relative humidity $\phi^*_{a,in,de}$ (equation (20)) achieved during dehumidification and maximum temperature ($T_{w,in,re}$) achieved during regeneration. These statements are deduced based on assertions made by researchers ([39,45,46]) for the case of desiccant wheels, wherein, in an ideal case, the minimum achievable relative-humidity of dehumidified air (at the outlet) equals the relative humidity (minimum) of the regeneration air-stream at the inlet whereas the maximum achievable relative-humidity of humidified air (at the outlet during regeneration) equals the relative humidity (maximum) of dehumidification air-stream at the inlet.

The aforementioned forms the basis of equations (22) and (23) which show the limiting minimum and maximum outlet humidity-ratio during dehumidification and regeneration, respectively. Note however that the mass-conservation principle has not yet been considered. We will do this next.

$$Y^*_{a,o,de} = Y(T_{w,in,de}, \phi^*_{a,in,re}) \tag{22}$$

$$Y^*_{a,o,re} = Y(T_{w,in,re}, \phi^*_{a,in,de}) \tag{23}$$

Under periodically-steady-state operation of the HMX, the reduction in the mass of moisture in the supply air-stream must be equal to the increase in mass of moisture in the regeneration air-stream. Assuming the time-period of dehumidification and regeneration to be equal, the following equality must hold.

$$\dot{m}_{a,de}(Y_{a,in,de} - Y_{a,o,de}) = \dot{m}_{a,re}(Y_{a,o,re} - Y_{a,in,re}) \tag{24}$$

Since equation (24) must be satisfied, the conditions of equations (22) and (23) need not always be achieved simultaneously. First, **if** the following condition holds:

$$\dot{m}_{a,de}(Y_{a,in,de} - Y^*_{a,o,de}) < \dot{m}_{a,re}(Y^*_{a,o,re} - Y_{a,in,re}) \tag{25}$$

then the maximum mass that can be exchanged by the two air-streams would be equal to the left-hand-side of the equation. The minimum value of the achievable specific-humidity of the dehumidification air-stream would then be given by equation (26), the right-hand-side of which is defined in equation (22).

$$Y_{a,o,de,min} = Y^*_{a,o,de} \tag{26}$$

However, the maximum outlet specific humidity achievable during regeneration would not be the same as $Y^*_{a,o,re}$ (as given by equation (23)), but should rather be deduced by invoking mass-conservation. Equation (27) gives the expression for the maximum outlet specific humidity.

$$Y_{a,o,re,max} = Y_{a,in,re} + \frac{\dot{m}_{a,de}}{\dot{m}_{a,re}}(Y_{a,in,de} - Y^*_{a,o,de}) \tag{27}$$

Note that the above limit is akin to the maximum/minimum temperature achievable by a perfect (ideal) heat exchanger when the thermal capacitance of the two heat-exchanging fluid-streams is not equal. While the fluid-stream (at the outlet of the heat exchanger) with a lower thermal capacitance reaches the inlet temperature of the fluid-stream with a larger thermal capacitance, the reverse is not true. Rather, the outlet temperature of the stream with larger thermal capacitance is derived using an energy conservation equation (see Incropera and DeWitt [43]).

The maximum mass transferred would be $M_{max} = \dot{m}_{a,de}\left(Y_{a,in,de} - Y_{a,o,de,min}\right) = \dot{m}_{a,re}\left(Y_{a,o,re,max} - Y_{a,in,re}\right)$

Thus, by equations (26) or (27),

$$M_{max} = \dot{m}_{a,de}(Y_{a,in,de} - Y^{*}_{a,o,de}) \quad (28)$$

Secondly, **if**

$$\dot{m}_{a,de}(Y_{a,in,de} - Y^{*}_{a,o,de}) > \dot{m}_{a,re}(Y^{*}_{a,o,re} - Y_{a,in,re}) \quad (29)$$

the maximum achievable moisture exchanged would be equal to the right-hand-side. In this case, equation (30) would hold.

$$Y_{a,o,re,max} = Y^{*}_{a,o,re} \quad (30)$$

By the mass conservation principle, the minimum outlet specific humidity achievable during dehumidification would be given by equation (31).

$$Y_{a,o,de,min} = Y_{a,in,de} - \frac{\dot{m}_{a,re}}{\dot{m}_{a,de}}(Y^{*}_{a,o,re} - Y_{a,in,re}) \quad (31)$$

The maximum mass transfer rate would be

$$M_{max} = \dot{m}_{a,de}\left(Y_{a,in,de} - Y_{a,o,de,min}\right) = \dot{m}_{a,re}\left(Y_{a,o,re,max} - Y_{a,in,re}\right) \quad (32)$$

Thus, by equations (30) or (31), $M_{max} = \dot{m}_{a,re}(Y^{*}_{a,o,re} - Y_{a,in,re})$ (33)

In summary, if equation (25) holds true, then by equations (26), (22) and (21)

$$Y_{a,o,de,min} = Y\left(T_{w,in,de}, \phi(T_{w,in,re}, Y_{a,in,re})\right) \quad (34)$$

Else if equation (29) holds true, then by equations (31), (23) and (20)

$$Y_{a,o,de,min} = Y_{a,in,de} - \frac{\dot{m}_{a,re}}{\dot{m}_{a,de}}\left(Y\left(T_{w,in,re}, \phi(T_{w,in,de}, Y_{a,in,de})\right) - Y_{a,in,re}\right) \quad (35)$$

Moreover, from equations (28), (32), (34) and (35).

$$M_{max} = min\left\{\dot{m}_{a,de}\left(Y_{a,in,de} - Y\left(T_{w,in,de}, \phi(T_{w,in,re}, Y_{a,in,re})\right)\right), \dot{m}_{a,re}\left(Y\left(T_{w,in,re}, \phi(T_{w,in,de}, Y_{a,in,de})\right) - Y_{a,in,re}\right)\right\} \quad (36)$$

Limiting values for the relative humidity for both dehumidification and regeneration air-streams can be evaluated using equations (37) and (38), after having evaluated $Y_{a,o,de,min}$ and $Y_{a,o,re,max}$.

$$\phi_{a,o,de,min} = \phi\left(T_{w,in,de}, Y_{a,o,de,min}\right) \quad (37)$$

$$\phi_{a,o,re,max} = \phi\left(T_{w,in,re}, Y_{a,o,re,max}\right) \quad (38)$$

3.3.3. Graphical method to determine the ideal performance

The outlet air-states can also be derived graphically and more intuitively on a psychrometric chart, as explained below and shown in Figure 3. The steps are analogous to those discussed in the previous section.

Steps:

i. Plot points D_i and R_i representing inlet air states during dehumidification and regeneration, respectively.
ii. Plot point D'_i such that $Y(D'_i) = Y(D_i)$ (same height in psychrometric chart) and $T(D'_i) = T_{w,in,de}$. Similarly, plot point R'_i such that $Y(R'_i) = Y(R_i)$ and $T(R'_i) = T_{w,in,re}$.
iii. Plot constant relative humidity lines $\phi^{*}_{a,in,de} = \phi(D'_i)$ and $\phi^{*}_{a,in,re} = \phi(R'_i)$.
iv. Plot point D^{*}_o such that $\phi(D^{*}_o) = \phi^{*}_{a,in,re}$ and $T(D^{*}_o) = T_{w,in,de}$. Similarly, plot point R^{*}_o such that $\phi(R^{*}_o) = \phi^{*}_{a,in,de}$ and $T(R^{*}_o) = T_{w,in,re}$.

If $\frac{D_i^{'}D_o^*}{R_i^{'}R_o^*} < \frac{\dot{m}_{a,re}}{\dot{m}_{a,de}}$ then $Y_{a,o,de,min} = Y(D^*_o)$, and $Y_{a,o,re,max} = Y(R^{**}_o)$. Here R^{**}_o is plotted such that $T(R^{**}_o) = T_{w,in,re}$ and

$R_i^{'}R_o^{**} = \frac{\dot{m}_{a,de}}{\dot{m}_{a,re}} D_i^{'}D_o^*$. Note that $\phi_{a,o,de,min} = \phi(D^*_o)$ and $\phi_{a,o,re,max} = \phi(R^{**}_o)$.

v. If $\frac{D_i^{'}D_o^*}{R_i^{'}R_o^*} > \frac{\dot{m}_{a,re}}{\dot{m}_{a,de}}$ then $Y_{a,o,re,max} = Y(R^*_o)$, and $Y_{a,o,de,min} = Y(D^{**}_o)$. Here R^{**}_o is plotted such that $T(D^{**}_o) = T_{w,in,de}$ and

$D_i^{'}D_o^{**} = \frac{\dot{m}_{a,re}}{\dot{m}_{a,de}} R_i^{'}R_o^*$. Note that $\phi_{a,o,de,min} = \phi(D^{**}_o)$, and $\phi_{a,o,re,max} = \phi(R^*_o)$.

vi. In a special case when $\frac{D_i^{'}D_o^*}{R_i^{'}R_o^*} = \frac{\dot{m}_{a,re}}{\dot{m}_{a,de}}$ then $Y_{a,o,de,min} = Y(D^*_o)$ and $Y_{a,o,re,max} = Y(R^*_o)$ as well as $\phi_{a,o,de,min} = \phi(D^*_o)$, and $\phi_{a,o,re,max} = \phi(R^*_o)$.

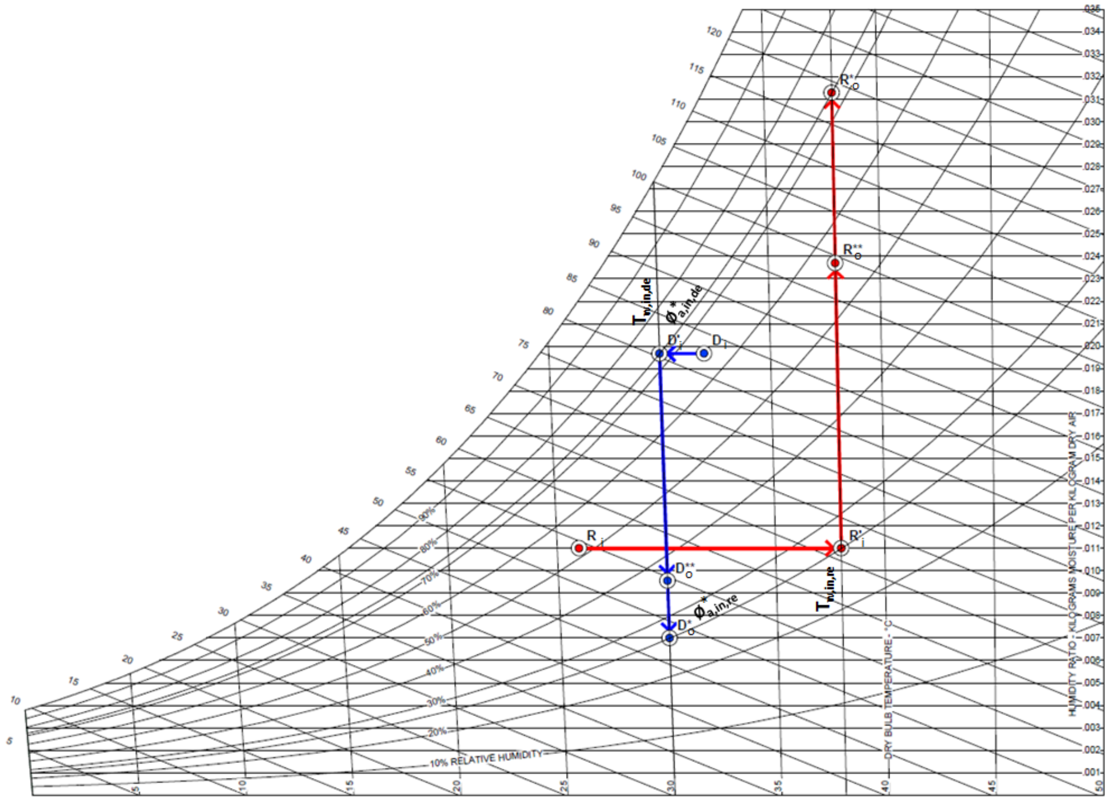

Figure 3: Psychrometric chart showing the graphical procedure to determine the maximum and minimum achievable humidity-ratio. The state-points D_i, R_i, D^*_o and R^*_o are based on conditions discussed in Section 5.2

3.4. *Expressions for humidity-ratio effectiveness and relative-humidity effectiveness*

Having obtained the heat and mass exchange for an ideal exchanger, we are now in a position to calculate the effectiveness factors ε_Y and ε_{RH}. Just as the temperature effectiveness is defined as (see Incropera and Dewitt [43])

$$\varepsilon_T = \frac{q_{actual}}{q_{max}} = \frac{C_h(T_{h,in} - T_{h,o})}{min\{C_c(T_{h,in} - T_{c,in}), C_h(T_{h,in} - T_{c,in})\}} = \frac{C_c(T_{c,o} - T_{c,in})}{min\{C_c(T_{h,in} - T_{c,in}), C_h(T_{h,in} - T_{c,in})\}},$$

the specific humidity effectiveness is defined as

$$\varepsilon_Y = \frac{M_{actual}}{M_{max}} = \frac{\dot{m}_{a,de}(Y_{a,in,de} - Y_{a,o,de})}{min\left\{\dot{m}_{a,de}\left(Y_{a,in,de} - Y^*_{a,o,de}\right), \dot{m}_{a,re}\left(Y^*_{a,o,re} - Y_{a,in,re}\right)\right\}}$$
$$= \frac{\dot{m}_{a,re}(Y_{a,o,re} - Y_{a,in,de})}{min\left\{\dot{m}_{a,de}\left(Y_{a,in,de} - Y^*_{a,o,de}\right), \dot{m}_{a,re}\left(Y^*_{a,o,re} - Y_{a,in,re}\right)\right\}} \tag{39}$$

as may be understood from equations (18), (24), (28) and (32). Also, the relative humidity effectiveness is

$$\varepsilon_{RH} = \frac{\phi^*_{a,in,de} - \phi_{a,o,de}}{\phi^*_{a,in,de} - \phi_{a,o,de,min}} = \frac{\phi(T_{w,in,de}, Y_{a,in,de}) - \phi(T_{a,o,de}, Y_{a,o,de})}{\phi(T_{w,in,de}, Y_{a,in,de}) - \phi(T_{w,in,de}, Y_{a,o,de,min})} \tag{40}$$

as may be understood from equations (19), (20) and (37).

Because $(dY/d\phi)|_T$ is larger at higher temperatures (constant RH lines are more dispersed at higher temperature on the psychrometric chart), for *equal* flow rates of dehumidification and regeneration air-streams (and equal process-times $t_1 = t_2$) we have $\dot{m}_{a,de}(Y_{a,in,de} - Y^*_{a,o,de}) < \dot{m}_{a,re}(Y^*_{a,o,re} - Y_{a,in,re})$. So for the common case of equal flow rates, the expressions for ε_Y and ε_{RH} can be simplified to

$$\varepsilon_Y = \frac{Y_{a,in,de} - Y_{a,o,de}}{Y_{a,in,de} - Y^*_{a,o,de}} \tag{41}$$

$$\varepsilon_{RH} = \frac{\phi^*_{a,in,de} - \phi_{a,o,de}}{\phi^*_{a,in,de} - \phi^*_{a,in,re}} = \frac{\phi(T_{w,in,de}, Y_{a,in,de}) - \phi(T_{a,o,de}, Y_{a,o,de})}{\phi(T_{w,in,de}, Y_{a,in,de}) - \phi(T_{w,in,de}, Y^*_{a,o,de})} \tag{42}$$

Notice that despite the similarities between the expressions for ε_T and ε_Y, a critical difference is that for ε_T the denominator is the difference between inlet temperatures of both the heat exchanging fluids ($T_{h,in} - T_{c,in}$) while for ε_Y it is either $(Y_{a,in,de} - Y^*_{a,o,de})$ or $(Y^*_{a,o,re} - Y_{a,in,re})$ and not $(Y_{a,in,de} - Y_{a,in,re})$. The reason for this difference is that heat transfer tends towards equalization of T (temperature) between fluid streams, while mass transfer via the desiccant in a mass regenerator tends towards equalization of relative humidity (subject to mass conservation, if the adsorption isotherm does not have hysteresis and is exclusively a function of relative humidity) and not the humidity-ratio (this observation is similar to that made by other researchers [31,39,45,46] as well), as can be seen from equation (42) wherein the denominator is $(\phi^*_{a,in,de} - \phi^*_{a,in,re})$.

4. Feasibility check and design methodology

4.1. Description

The comprehensive heat and mass transfer model described in Section 2 requires a reasonable degree of time and numerical skills to implement and use. Instead of adopting a trial-and-error approach of designing an HMX using the comprehensive model, here we will describe an approximate design methodology. The methodology is in the form of a simple and non-iterative calculation procedure, allowing the design of an HMX to achieve a desired target specific humidity of the treated air-stream, given the inlet conditions and flow rates of air and water streams. The methodology by itself, at the least, provides a reasonable estimate of the HMX design parameters required to approximately achieve the target outlet specific humidity of the dehumidified air; if however a higher precision is required, either a good estimate of the correction factor (tuning parameter) C_f is necessary or else the comprehensive model must be used.

The mass of moisture that the coated desiccant can adsorb (given the inlet conditions and flow rates of air and water streams) is among the most significant factors that determine the performance of the HMX in terms of outlet specific humidity of the dehumidified air. Hence, the design methodology primarily focuses on ensuring the availability of enough desiccant to dehumidify air to a required moisture-content. The following two conditions determine whether the HMX can deliver the targeted outlet specific humidity of the dehumidified air.

Condition 1: The required outlet specific humidity of a real HMX cannot be lower than that of an ideal HMX (section 3). Thus, the condition given by equation (43) must be satisfied.

$$Y_{r,in} > Y_{a,o,de,min} \tag{43}$$

Note that if the HMX is to completely handle the latent heat in a system represented in Figure 1, the target outlet specific humidity would be the room inlet specific humidity $Y_{r,in}$.

Condition 2: A real HMX may have a substantial thermal mass. Thus, the main concentration wave front (during which the desired substantial dehumidification occurs) is preceded by a thermal wave front driven by the heat stored in the HMX from the previous regeneration process (see Mei et al.[47] for more details). Poor performance during the prevalence of the thermal wave front (because the outlet specific humidity $Y_{a,o,de\text{-}tw,avg}$ can be quite high) makes it necessary that the performance during the prevalence of the concentration wave compensates for this. Thus, the average outlet humidity of dehumidified air during the concentration-wave ($Y_{a,o,de\text{-}cw,avg}$) needs to be somewhat lower than the target specific humidity required. This may be realized from equation (44). Note that dehumidification process time is subdivided into two sub-periods t_{tw} and t_{cw} which denote the time period of the thermal wave and the concentration wave, respectively. Furthermore, a real HMX cannot be expected to have an effectiveness approaching 1. For design purposes, an effectiveness of 0.85 is considered to be the limiting value which would result in a minimum achievable specific humidity value of $Y_{a,o,de,min\text{-}real}$ (larger than $Y_{a,o,de,min}$). Condition 2, expressed by equation (46), must therefore be satisfied.

$$Y_{r,in} = \frac{t_{tw}}{t_1} Y_{a,o,de-tw,avg} + \frac{t_{cw}}{t_1} Y_{a,o,de-cw,avg} \tag{44}$$

where $t_1 = t_{tw} + t_{cw}$ (45)

$$Y_{a,o,de-cw,avg} > Y_{a,o,de,min-real} \tag{46}$$

For a periodically steady-state condition, by mass conservation, the moisture to be removed from air during the dehumidification process must equal the increase in sorbate uptake, as shown in equation (47), where $W(\phi_{final})$ and $W(\phi_{initial})$ are the spatially-averaged sorbate uptakes (assumed to be functions of the relative humidity of the air within the desiccant pores) at the end (final state) and beginning (intial state) of the dehumidification process, respectively.

$$m_a \left(Y_{a,in,de} - Y_{r,in} \right) = m_d \left(W(\phi_{final}) - W(\phi_{initial}) \right) \tag{47}$$

Here the mass of air and mass of desiccant material are given by

$$m_a = \rho_{a,dry} A_a U_{a,de} t_1 ,\ A_a = L_y L_z ,\ m_d = \rho_d (1-\varepsilon_d) H_d A_{d,total} \tag{48}$$

with a total desiccant area

$$A_{d,total} \approx \frac{2L_z}{P_f} \left(L_x L_y - \frac{L_x L_y}{X_l X_t} \frac{\pi d_o^2}{4} \right) \tag{49}$$

Equations (47) to (49) yield an expression for the ratio of the total length of the fin to the fin pitch, equation (50).

$$\frac{L_x}{P_f} \approx \frac{C_f \rho_{a,dry} U_{a,de} (Y_{a,in,de} - Y_{r,in}) t_1}{\rho_d (1-\varepsilon_d) H_d \left(W(\phi_{final}) - W(\phi_{initial}) \right)} \frac{2 X_l X_t}{\left(4 X_l X_t - \pi d_o^2 \right)} \tag{50}$$

Since the estimation of $W(\phi_{final})$ and $W(\phi_{initial})$, described further in this section, is for an ideal case of negligible mass-transfer resistance, it would lead to over-estimation of the sorbate uptake during the dehumidification process. Therefore, the difference in sorbate uptake is divided by a correction factor (tuning parameter) C_f, whose value is expected to be larger than 1. The higher the value of C_f, the larger the necessary ratio of the fin length to the fin pitch (L_x/P_f) and the larger would be the desiccant area $A_{d,total}$.

The fin length to fin pitch ratio L_x/P_f is considered to be the most important geometrical design parameter of the HMX. The tube longitudinal and transversal pitch X_l, X_t as well as tube inner and outer diameter d_i and d_o may be chosen based on their typical values for standard fin-tube heat exchangers (see Table 3). Having fixed the desiccant, the desiccant density ρ_d, porosity ε_d and adsorption isotherm ($W = W(\phi)$) are known. H_d may be chosen based on a realistic desiccant coating thickness (250 μm in the present case). The flow cross-section A_a (= $L_y L_z$) may be chosen such that it results in an air velocity $U_{a,de}$ of 2 m/s, typical for the air velocity across cooling coils in air handling units. t_1 may be chosen based on realistic values such as those encountered in desiccant wheels. Given the inlet air-states, $Y_{a,in,de}$ is known and the target HMX outlet humidity (which is the same as the room-inlet humidity) $Y_{r,in}$ is known too (values are given in Table 4). Thus, to evaluate L_x/P_f, the only remaining unknowns are $W(\phi_{initial})$ and $W(\phi_{final})$.

The spatially averaged sorbate uptake $W(\phi_{final})$ at the end (final time-instant) of the dehumidification process is assumed to be the average of sorbate uptake of the desiccant near the inlet and outlet of the dehumidification air-stream at the end of the process, as shown in equation (51). The sorbate uptake values are a function of the respective relative humidity values. The relative humidity values in turn can be expressed as functions of the temperature of the desiccant and specific humidity of air in the vicinity of the desiccant. In the interest of simplifying the calculations, relative humidity is expressed as a function of time and spatially averaged water temperature and specific humidity in the air-stream at the location of interest.

$$W(\phi_{final}) = \frac{W(\phi_{a,in,de,final}) + W(\phi_{a,o,de,final})}{2} \tag{51}$$

Here,

$$\phi_{a,in,de,final} = \phi\left(T_{w,de}, Y_{a,in,de} \right) \tag{52}$$

$$\phi_{a,o,de,final} = \phi\left(T_{w,de}, Y_{r,in} \right) \tag{53}$$

The time and spatially averaged water temperature during the dehumidification process $T_{w,de}$ (equation (54)) can be derived using the approximate energy-conservation law expressed by equation (55). Note that this is the water-temperature expected to prevail during the concentration-wave (after the passage of the thermal-wave). Thus, the thermal-capacitance of the HMX is not accounted for. Also note that for the second term on the right-hand-side, it is assumed that the outlet air-temperature approaches $T_{w,de}$. Since the average temperature is assumed to be the arithmetic mean of inlet and outlet temperature (see equation (8) of the supplementary material), it can be inferred that ($T_{w,o,de}$ - $T_{w,in,de}$) = 2($T_{w,de}$ - $T_{w,in,de}$). Rearranging terms yields equation (56).

$$T_{w,de} = \frac{1}{t_1}\int_{t_1}^{t_1+t_2} T_{w,s-avg,de}\,dt \tag{54}$$

$$2\dot{m}_{w,c}C_{p,w}\left(T_{w,de}-T_{w,in,de}\right)t_1 \approx \rho_{a,dry}A_aU_{a,de}q_{eva}\left(Y_{a,in,de}-Y_{r,in}\right)t_1+\rho_aA_aU_{a,de}C_p\left(T_{a,in,de}-T_{w,de}\right)t_1 \tag{55}$$

$$T_{w,de} \approx \frac{\rho_{a,dry}A_aU_{a,de}q_{eva}\left(Y_{a,in,de}-Y_{r,in}\right)+\rho_aA_aU_{a,de}C_{p,a}T_{a,in,de}+2\dot{m}_{w,c}C_{p,w}T_{w,in,de}}{\rho_aA_aU_{a,de}C_{p,a}+2\dot{m}_{w,c}C_{p,w}} \tag{56}$$

Equations (57) to (62) are used to derive $W(\phi_{initial})$. These are analogous to equations (51) to (56). Note that the initial values of sorbate uptake (at the start of the dehumidification process) depend on the prevailing temperature and humidity conditions at the end of the previous regeneration process. Hence, as may be seen in equations (58) and (59), the relative humidity near the inlet and outlet (defined with respect to the direction of flow of dehumidification air-stream) are dependent on the relative humidity at the outlet and inlet during the regeneration process, respectively, and the prevailing spatially and temporally averaged water temperature $T_{w,re}$ during the regeneration process.

$$W(\phi_{initial}) = \frac{W(\phi_{a,in,de,initial})+(\phi_{a,o,de,initial})}{2} \tag{57}$$

$$\phi_{a,in,de,initial} = \phi\left(T_{w,re},Y_{a,o,re,avg}\right) \tag{58}$$

$$\phi_{a,o,de,initial} = \phi\left(T_{w,re},Y_{a,in,re}\right) \tag{59}$$

$$T_{w,re} = \frac{1}{t_2}\int_0^{t_2} T_{w,s-avg,re}\,dt \tag{60}$$

$$2\dot{m}_{w,h}C_{p,w}\left(T_{w,re}-T_{w,in,re}\right)t_2 \approx \rho_{a,dry}A_aU_{a,re}q_{eva}\left(Y_{a,o,re,avg}-Y_{a,in,re}\right)t_2+\rho_aA_aU_{a,re}C_p\left(T_{w,re}-T_{a,in,re}\right)t_2 \tag{61}$$

Just as it is assumed that ($T_{w,o,de}$ - $T_{w,in,de}$) = 2($T_{w,de}$ - $T_{w,in,de}$), it is similarly assumed that ($T_{w,o,re,avg}$ - $T_{w,in,re}$) = 2($T_{w,re}$ - $T_{w,in,re}$). For the second term on the right-hand-side of equation (61), it is assumed that the outlet air-temperature approaches $T_{w,re}$. Rearranging terms yields equation (62).

$$T_{w,re} \approx \frac{\rho_{a,dry}A_aU_{a,re}q_{eva}\left(Y_{a,o,re,avg}-Y_{a,in,re}\right)+\rho_aA_aU_{a,re}C_{p,a}T_{a,in,re}+2\dot{m}_{w,h}C_{p,w}T_{w,in,re}}{\rho_aA_aU_{a,re}C_{p,a}+2\dot{m}_{w,de}C_{p,w}} \tag{62}$$

By mass-conservation, equation (63) must hold. Hence, the first term in the numerator of equation (62) may be substituted by the right-hand-side term of equation (63), since the latter is known *a priori* while the former is not.

$$\rho_{a,dry}A_aU_{a,re}\left(Y_{a,o,re,avg}-Y_{a,in,re}\right)t_2 = \rho_{a,dry}A_aU_{a,de}(Y_{a,in,de}-Y_{r,in})t_1 \tag{63}$$

Recalling the aforementioned condition 2, the following equations (64) to (73) help test whether $Y_{a,o,de\text{-}cw,\mathrm{avg}} > Y_{a,o,de,min\text{-}real}$ holds true. $Y_{a,o,de\text{-}cw,\mathrm{avg}}$ may be evaluated from equation (44), while $Y_{r,in}$ and t_1 are known. t_{tw} and t_{cw} are related by equation (45). Thus, to evaluate $Y_{a,o,de\text{-}cw,\mathrm{avg}}$, we must first be able to evaluate t_{tw} and $Y_{a,o,de\text{-}tw,\mathrm{avg}}$. Equation (64) approximates $Y_{a,o,de\text{-}tw,\mathrm{avg}}$ as the arithmetic mean of inlet specific humidity of the regeneration air stream $Y_{a,in,re}$ (since this is the specific humidity value that the desiccant is exposed to, near the outlet of the dehumidification air-stream, at the beginning of the dehumidification process) and the average outlet specific humidity during dehumidification $Y_{r,in}$ (since this is the expected value at the end of the thermal wave). Note that, since this is a counter-flow HMX, the air-inlet cross-section during regeneration is the same as the air-outlet cross-section during dehumidification, which explains the use of $Y_{a,in,re}$ instead of $Y_{a,o,re}$. The arithmetic mean implies that an approximately linear time dependence of the outlet specific humidity from $Y_{a,in,re}$ to $Y_{r,in}$ is assumed during the thermal wave of the dehumidification process.

$$Y_{a,o,de-tw,avg} = \frac{Y_{a,in,re}+Y_{r,in}}{2} \tag{64}$$

A time-dependent energy conservation equation, during the prevalence of thermal wave (from time *0* to t_{tw}) is given in equation (65). The heat taken up by water (left-hand-side) is equal to the sum of the rate of decrease in internal energy of the HMX, the sorption heat released and the decrease in enthalpy of the air-stream from inlet to outlet. Simplifications involved are: (i) the outlet air-temperature is assumed to be equal to the spatially-averaged water temperature, (ii) q_{ads} is assumed to be equal to its lower limit, q_{eva}, which leads to a slight underestimation of the heat source term, and (iii) the difference in specific humidity is assumed to be constant ($Y_{a,in,de} - Y_{r,in}$) throughout the time-period of the thermal wave, which leads to a slight over-estimation of the heat source term. Moreover, since the average temperature is assumed to be the arithmetic mean of inlet and outlet temperature (see equation (8) of the supplementary material), it follows that ($T_{w,o,de}(t)$ - $T_{w,in,de}$) = 2($T_{w,s\text{-}avg,de\text{-}tw}(t)$ - $T_{w,in,de}$).

$$2\dot{m}_w C_{p,w}\left(T_{w,s-avg,de-tw}(t)-T_{w,in,de}\right)=-(mC_p)_{HMX}\frac{dT_{w,s-avg,de-tw}}{dt}+ \rho_a A_a U_{a,de} q_{eva}\left(Y_{a,in,de}-Y_{r,in}\right)+\rho_a A_a U_{a,de} C_{p,a}\left(T_{a,in,de}-T_{w,s-avg,de-tw}(t)\right) \tag{65}$$

Here, the total thermal capacitance of the HMX equals the sum of the thermal capacitance of the desiccant, fins, tubes as well as the water inside the tubes.

$$(mC_p)_{HMX}=(1-\varepsilon_d)\rho_d A_{d,total} H_d C_{p,d}+\rho_f A_{d,total} H_f C_{p,f}+\rho_t\frac{\pi}{4}\left(d_{1,o}^2-d_{1,i}^2\right)L_z N_t C_{p,t}+\rho_w\frac{\pi d_{1,i}^2}{4}L_z N_t C_{p,w} \tag{66}$$

Rearranging the terms reduces equation (65) to the form

$$\frac{d\theta}{dt}+\lambda\theta=0 \tag{67}$$

were $\theta=T_{w,s-avg,de-tw}(t)-T_{ref}$, (68)

$$\lambda=\frac{2\dot{m}_w C_{p,w}+\dot{m}_a C_{p,a}}{(mC_p)_{HMX}} \ , \tag{69}$$

and

$$T_{ref}=\frac{2\dot{m}_w C_{p,w} T_{w,in,de}+\rho_a A_a U_{a,de} C_{p,a} T_{a,in,de}+\rho_a A_a U_{a,de} q_{eva}\left(Y_{a,in,de}-Y_{r,in}\right)}{\left(2\dot{m}_w C_{p,w}+\rho_a A_a U_{a,de} C_{p,a}\right)}. \tag{70}$$

Note that $T_{ref} = T_{w,de}$ (see equation (56)).

Equation (67) can be solved analytically, yielding

$$t_{tw}=-\frac{1}{\lambda}\ln\frac{\theta_{tw}}{\theta_0} \tag{71}$$

This solution implies that it would take infinite time for $T_{w,s\text{-}avg.de\text{-}tw}(t)$, whose initial value is $T_{w,re}$, to approach T_{ref} (= $T_{w,de}$). This is due to the simplifying assumptions that resulted in equation (65). Assuming that, practically speaking, $\theta_{tw}= T_{w,s\text{-}avg.de\text{-}tw}(t_{tw})$- T_{ref} approaching 0.5ºC would imply the end of the thermal-wave, equation (71) simplifies to equation (72).

$$t_{tw}=-\frac{1}{\lambda}\ln\frac{0.5}{\theta_0}=-\frac{1}{\lambda}\ln\frac{0.5}{T_{w,re}-T_{w,de}} \tag{72}$$

$Y_{a,o,de\text{-}cw,\mathrm{avg}}$ may thus be evaluated using equations (44), (45), (64) and (72), and checked whether it is larger than $Y_{a,o,de,min\text{-}real}$ as shown in equation (73), using the assumed effectiveness ε_Y = 0.85. It may be noted that while effectiveness values larger than 0.85 are possible, it would generally imply the availability of a large surface area, which implies a very large L_x and a very small P_f. This would be quite impractical from the point of view of bulkiness, and lead to a high blower fan power requirement.

$$Y_{a,o,de,min-real}=Y_{a,in,de}-\varepsilon_Y\left(Y_{a,in,de}-Y_{a,o,de,min}\right) \tag{73}$$

4.2. Summary

To summarize the procedure for designing an HMX, the steps mentioned in Table 1 or the flow-chart given in Figure 4 can be followed, given (or assuming) the geometrical values (X_l, X_t, d_i, d_o, ρ_d, ε_d), adsorption isotherm ($W = W(\phi)$), desiccant thickness H_d, air velocities $U_{a,de}$, $U_{a,re}$, times t_1, t_2, the target outlet humidity of the dehumidified air ($Y_{r,in}$), and the inlet states of water and air-streams.

Table 1: Steps for the design of an HMX

Step No.	Variable/Condition	Equation(s)	Comment
1	$Y_{a,o,de,min}$	(26) or (31)	Depending on whether condition (25) or (29) is satisfied.
2	Condition 1	(43)	Proceed only if true, else HMX cannot deliver the target value unless the given inlet conditions of air and/or water-streams are changed.
3	$T_{w,de}$ (or T_{ref})	(56)	
4	$T_{w,re}$	(62), (63)	
5	λ	(66), (69)	
6	t_{tw}	(72)	
7	$Y_{a,o,de\text{-}tw,avg}$	(64)	
8	$Y_{a,o,de\text{-}cw,avg}$	(44), (45)	
9	$Y_{a,o,de,min\text{-}real}$	(73)	
10	Condition 2	(46)	Proceed only if true, else HMX cannot deliver the target value unless one or more of the assumed variables (such as flow-rates, t_1, t_2) are changed.
11	$Y_{a,o,re,avg}$	(63)	
12	$W(\varphi_{final})$	(51),(52),(53)	
13	$W(\varphi_{initial})$	(57),(58),(59)	
14	L_x/P_f	(50)	
15	C_f	-	Correction factor value; may be selected based on experience.

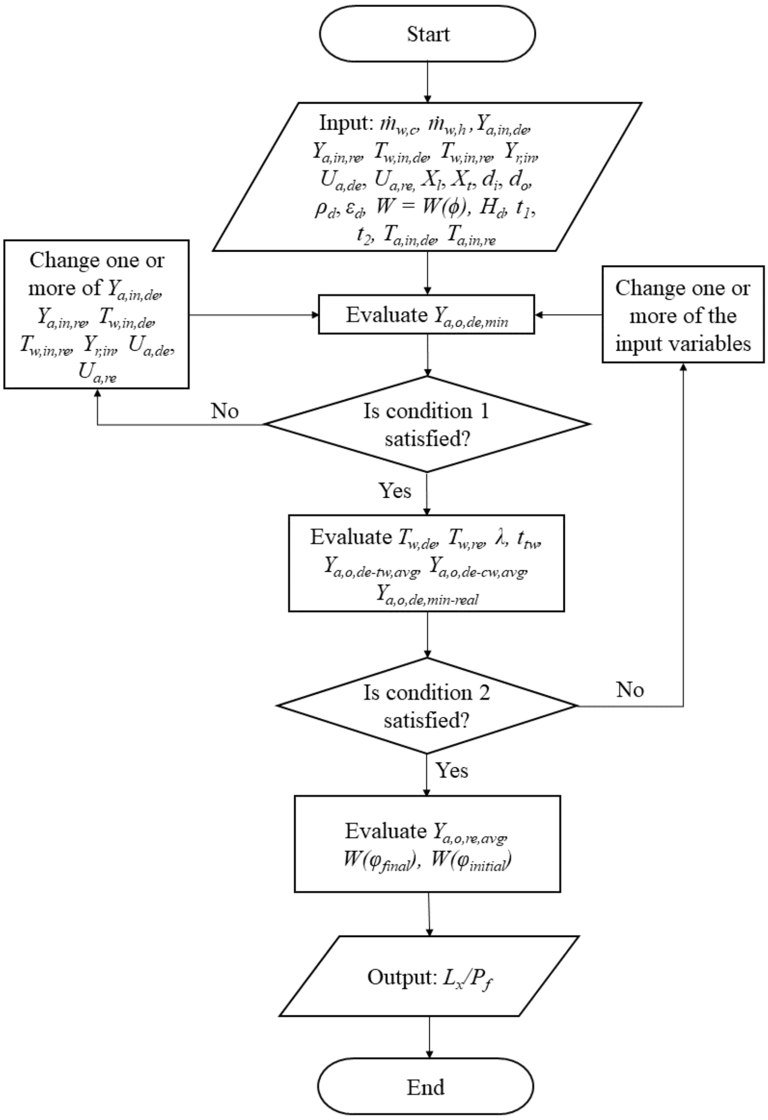

Figure 4: Flow-chart summarizing the feasibility check and design methodology

5. Results and discussion

5.1. Validation of the heat and mass transfer model

Simulation results of the heat and mass transfer model are compared with the experimental results of Oh et al. [7], who used a fin tube heat exchanger coated with 0.1 mm thick RD type silica gel on its fins. Cool water at 30°C and hot water at 80°C was used during dehumidification and regeneration, respectively. Oh et al. plotted the average dehumidification, maximum dehumidification and thermal coefficient of performance for various air flow rates, inlet air temperatures as well as inlet air relative humidities. Input parameters to the simulation model were set in accordance with the experimental conditions. It was assumed that the desiccant isotherm is independent of temperature; Oh et al. showed that the isotherm varies only very weakly with temperature [7]. A correlation for the temperature-averaged isotherm is given by equation (74).

$$W = 1.276\phi_d^6 + 3.739\phi_d^5 - 13.809\phi_d^4 + 12.192\phi_d^3 - 3.809\phi_d^2 + 0.830\phi_d \qquad (74)$$

In Figure 5, colored dots represent our simulation results while the black dots connected with lines represent the experimental data. Note that *De* is the amount of moisture removed, i.e. difference between inlet and outlet specific humidity, while COP_{th} is given by equation (75) (as suggested by Oh et al. [24]).

$$COP_{th} = \frac{\dot{m}_a q_{eva}(Y_{a,in,de} - Y_{a,o,de,avg})}{\dot{m}_w C_{p,w}(T_{w,in,re} - T_{w,o,re})} \qquad (75)$$

Figure 5 shows that all three variables (average dehumidification, maximum dehumidification and thermal COP) under various operating conditions are well predicted by our heat and mass transfer model, validating our model. Slight variations for some of the data points may be due to some of the simplifying assumptions used to develop our model as well as certain unavoidable experimental issues such as heat loss and effects due to thermal capacitance of ducts and pipe sections that are upstream of the desiccant coated HX.

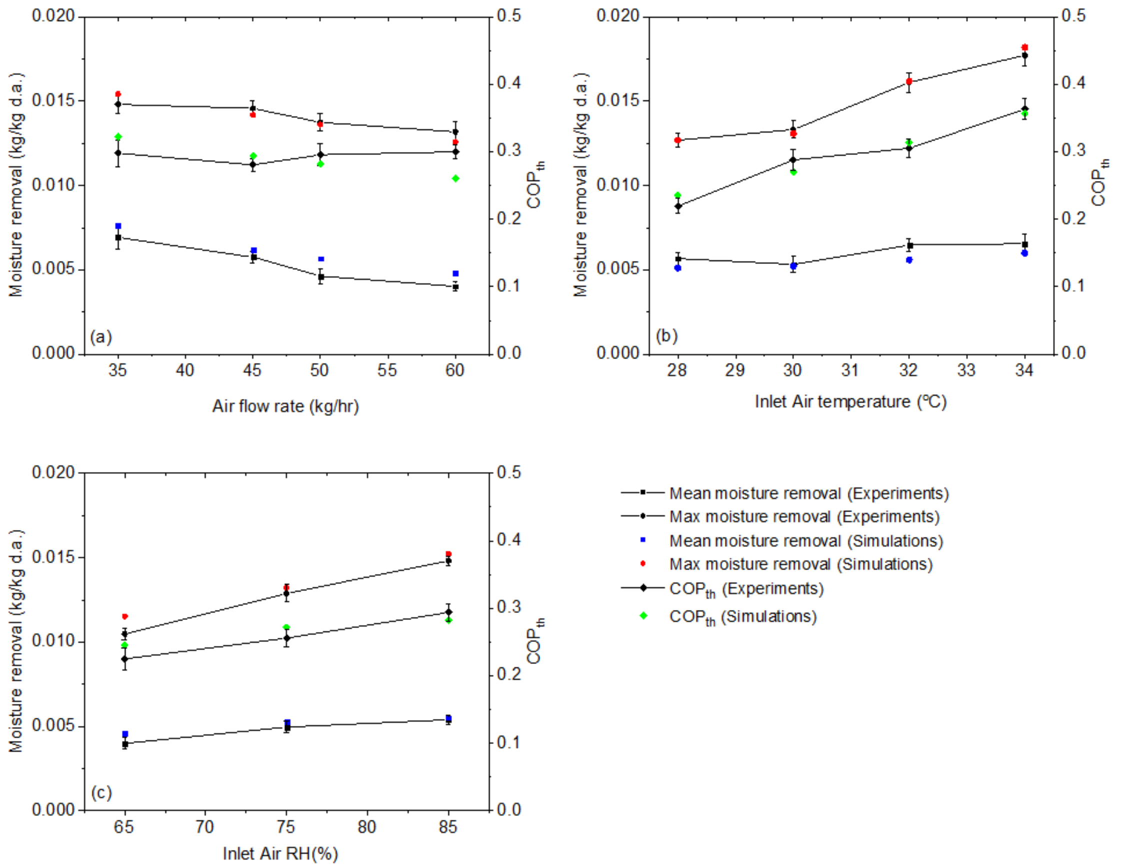

Figure 5: Comparison between simulation and experimental results by Oh et al. [7] for moisture removal De (in kg per kg dry air, left scale) and thermal coefficient of performance (right scale) versus (a) air-flow rate, (b) inlet air temperature, and (c) inlet air relative humidity.

5.2. Validation of the performance of the ideal heat and mass exchanger

Next, we validate the performance of an ideal HMX by comparing the theoretical predictions from section 3 with simulations using idealized or close-to-ideal parameters and variables, as explained in Table 2. Desiccant properties as well as some of the geometrical parameters are shown in Table 3. Inlet conditions of hot and cool water are 38^{o}C and 30^{o}C, respectively. The dehumidification air-stream (ambient air) inlet is 32^{o}C at 65% relative humidity ($Y_{a,in,de}$ = 0.0197 kg/kg dry air) and the regeneration air-stream (room-return air) is 25^{o}C at 55% relative humidity ($Y_{a,in,re}$ = 0.011 kg/kg dry air).

Table 2: Input data to simulate a close-to-ideal ICHDMX

Parameter	**Value**	**Comment**
$\eta_{f,app}$	1	These values ensure negligible heat and mass transfer resistance on the fin and fluid side.
h_w	10^5 W/(m^2-K)	
h_a	10^3 W/(m^2-K)	
$h_{a,m}$	1 m/s	
H_d	50 µm	This ensures a small non-dimensional diffusion time (Fourier number) as well as small heat and mass transfer resistance on the desiccant side.
P_f	1 mm	These values ensure a very large heat and mass transfer area and a large quantity of desiccant.
L_x	0.044-1.1 m	
$C_{p,f}$	0.1 J/(kg-K)	These values ensure negligible thermal mass of the system.
$C_{p,t}$	0.1 J/(kg-K)	
$C_{p,d}$	0.1 J/(kg-K)	
M_w	0.1 kg	
$T_{w,avg}$	$T_{w,in}$	Imposing this condition instead of implementing equation (6) mimics the performance of fluid flow with infinite thermal capacity and a negligible tube volume, i.e. terms ψ_9 and ψ_{10} are negligible.
t_1, t_2	90 s	Small values for the time-period and air-flow velocities ensure that a large amount of desiccant is available for adsorption (desorption) throughout the process compared to the total amount of moisture to be removed (added) from (to) air during dehumidification (regeneration).
$U_{a,de}$	0.5 m/s	
$U_{a,re}$	-0.5, -0.25 m/s	

Table 3: Desiccant properties and geometrical parameters of the HMX

Desiccant properties					
ρ_d	1167 kg/m^3	f_d	0.9	$C_{p,d}$	0.921 kJ/(kg.K)
ε_d	0.3	υ_r	2 nm		
HMX dimensions					
X_l	21 mm	L_y	0.6 m	H_f	0.1 mm
X_t	25 mm	$d_{t,o}$	9.5 mm	H_d	0.25 mm
L_z	1.2 m	$d_{t,i}$	8.5 mm		

Two cases are simulated (i) $U_{a,de} = - U_{a,re}$ = 0.5 m/s (satisfying the condition given by equation (25)) and (ii) $U_{a,de}$ = -2 $U_{a,re}$ = 0.5 m/s (satisfying the condition given by equation (29)). The number of rows N_r of the HMX is varied from 2 to 50 (i.e. the depth of the HMX varies from L_x = 0.044 to 1.1 m). With increase in N_r the surface area increases, implying an increase in availability of the desiccant mass available for adsorption. Figure 6(a)-(e) shows the approach to ideal behaviour for case (i), where $Y_{a,o,de,avg}$ and $Y_{a,o,re,avg}$ approach $Y_{a,o,de,min}$ and $Y_{a,o,re,max}$ (evaluated using equations (26) and (27)), while $\phi_{a,o,de,avg}$ and $\phi_{a,o,re,avg}$ approach $\phi_{a,o,de,min}$ and $\phi_{a,o,re,max}$ (evaluated using equations (37) and (38)), respectively, as N_r increases. Consequently, the value of ε_Y as well as ε_{RH} approach 1 (evaluated using equations (39) and (40)). The results are analogous for case (ii) as seen in Figure 7(a)-(e). Thus, the simulation results verify that the methods described in section 3 correctly determine the limiting performance of an ideal HMX and that these may be used as a reference (ideal performance) for defining ε_Y and ε_{RH}.

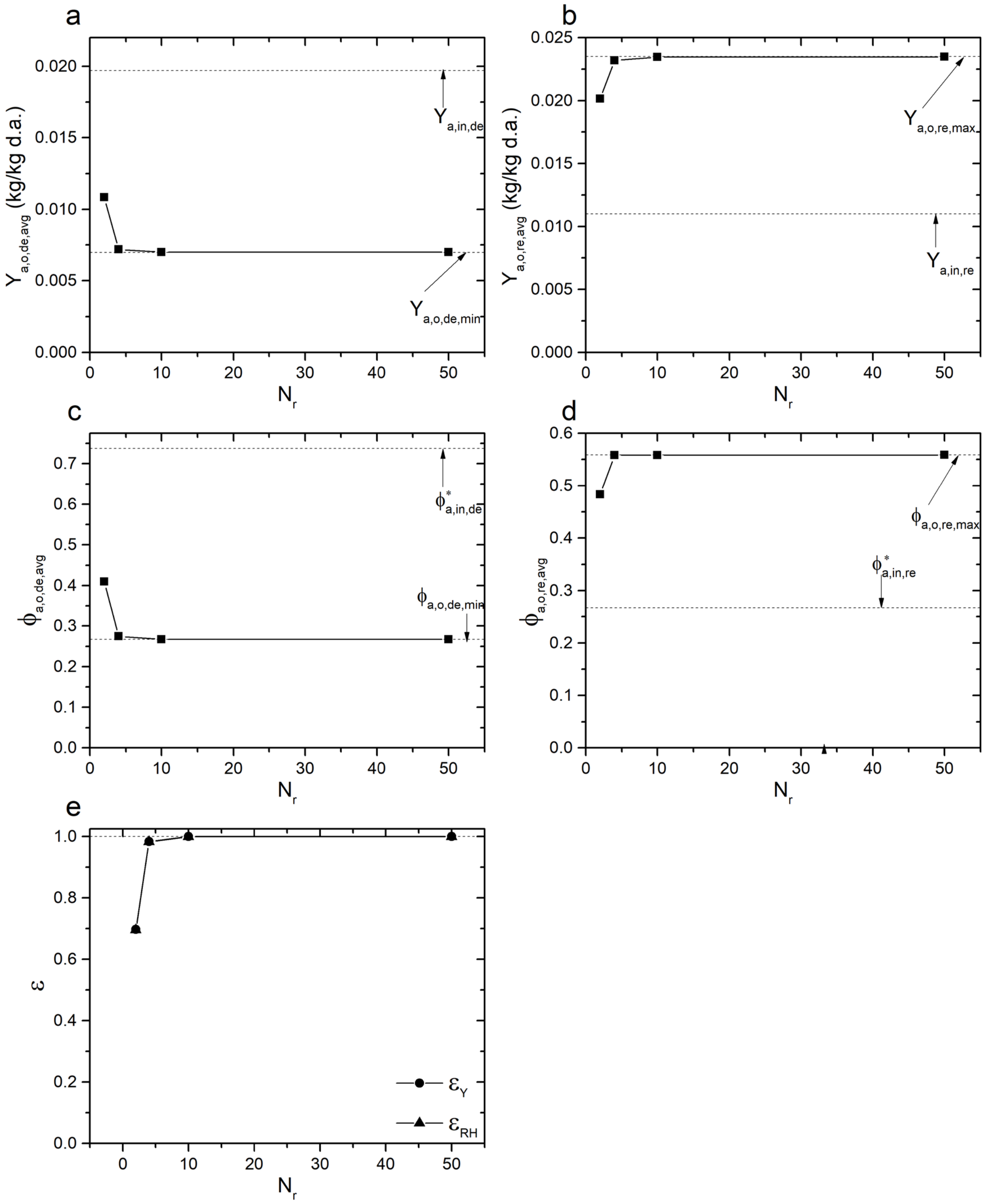

Figure 6: Approach to ideal performance for the case $U_{fr,1} = -U_{fr,2} = 0.5$ m/s. (a) $Y_{a,o,de,avg}$ versus N_r, (b) $Y_{a,o,re,avg}$ versus N_r, (c) $\phi_{a,o,de,avg}$ versus N_r, (d) $\phi_{a,o,re,avg}$ versus N_r, (e) ε_Y, ε_{RH} versus N_r.

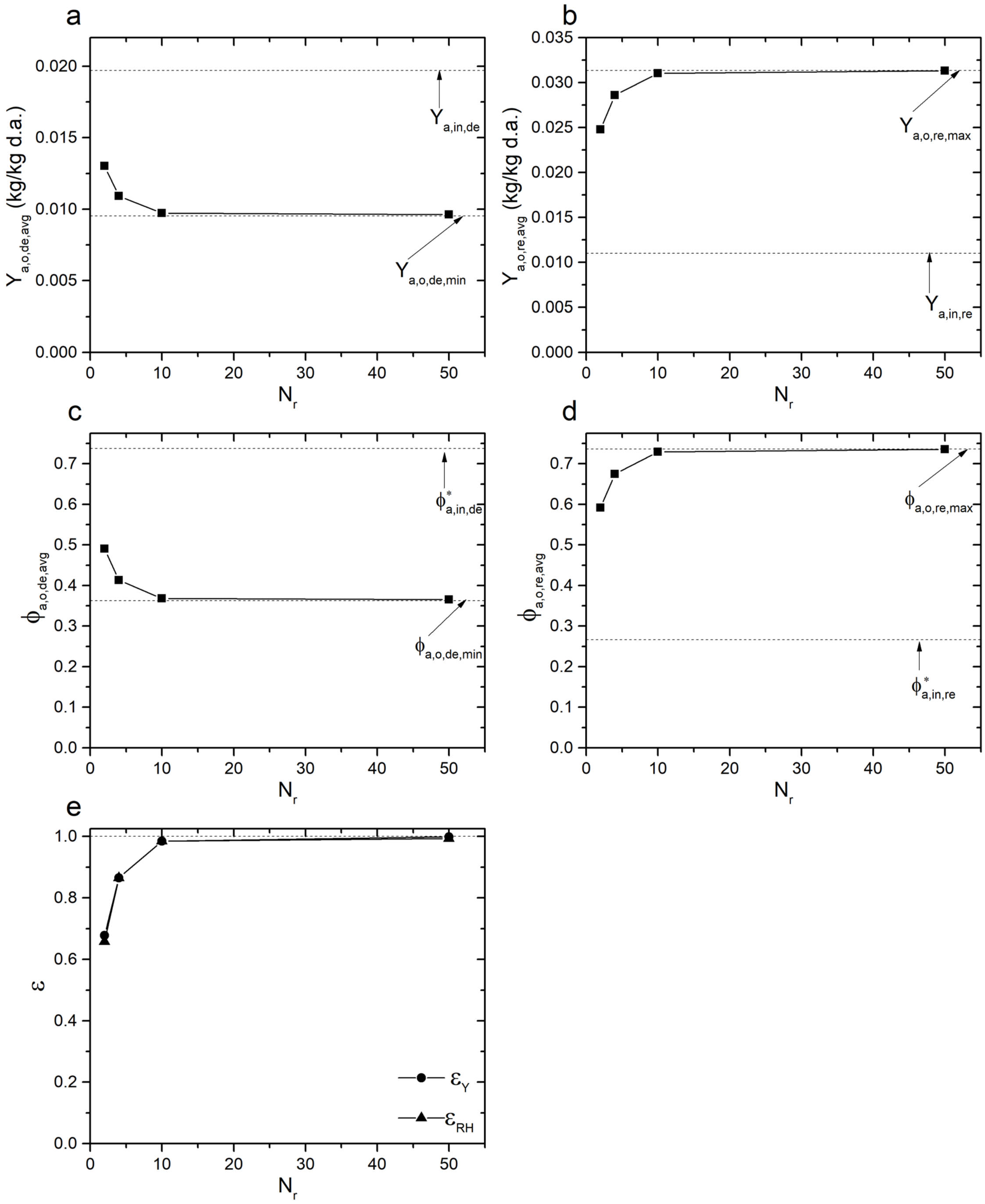

Figure 7: Approach to ideal performance for $U_{fr,1} = -2U_{fr,2} = 0.5$ m/s. (a) $Y_{a,o,de,avg}$ versus N_r, (b) $Y_{a,o,re,avg}$ versus N_r, (c) $\phi_{a,o,de,avg}$ versus N_r, (d) $\phi_{a,o,re,avg}$ versus N_r, (e) ε_Y, ε_{RH} versus N_r.

5.3. Performance analysis of a real HMX and demonstration of design methodology

With the validation of the comprehensive heat and mass transfer model and establishment of proper definitions of ideal performance, we can now use the model to analyse the performance of a real HMX, and to demonstrate the design methodology. The value for L_x/P_f is first evaluated using the design methodology described in Section 4 by first assuming C_f = 1. A reasonable value of L_x (very large values may be avoided since it may result in excessive bulkiness) is then chosen, which may be a multiple of X_l, such that the value of P_f too is reasonable (neither too large so as to avoid drastic reduction in heat and mass transfer coefficients, nor too small so as to avoid excessive pressure drop and the consequent large blower fan power consumption). L_x as well as the evaluated P_f are then used as an input to the comprehensive model discussed in section 2. The value of C_f is then incremented in steps of 0.1 and the aforementioned procedure is continued until the simulation derived average outlet specific humidity during dehumidification $Y_{a,o,de,avg}$ equals the target value $Y_{r,in}$.

The operating conditions are given in Table 4, and the geometrical parameters as well as the desiccant properties are given in Table 3. Table 5 gives details regarding the cases tested. Three hot water inlet temperatures $T_{w,in,re}$ (used during regeneration) were studied at 38, 44 and 50ºC, implying a temperature difference between cool water inlet (used during dehumidification) and hot water inlet of just 8, 14 and 20ºC, respectively. For each of the hot water temperatures, five cases were considered for different mixing ratios of fresh-air and room-return air. This results in inlet dehumidification / regeneration air-streams' temperature and specific-humidity ranging from 25 to 32ºC and 0.011 to 0.02 kg/kg dry air, respectively. Thus, a reasonably wide range of conditions are studied. Table 5 also shows the values of variables evaluated (starting from column titled $Y_{a,o,de,min}$) in the same order as the steps mentioned in

Table 1 for determining the feasibility of an HMX and designing it. For $T_{w,in,re}$ of 38, 44 and 50ºC, the chosen optimal L_x was 1.008 m, 0.504 m and 0.210 m, respectively.

For the lowest hot water inlet temperature $T_{w,in,re}$ = 38ºC, for cases no. 1, 2 and 3, condition 1 is not satisfied since $Y_{a,o,de,min}$ is larger than the target specific humidity of the dehumidified air $Y_{r,in}$. Based on the developed concept of an ideal HMX and verification of its performance in the previous section, it is clear that the outlet specific humidity in case of a real HMX cannot go below $Y_{a,o,de,min}$, thus the HMX would not be able to handle the complete moisture load. Simulations are hence not conducted under these conditions. Condition 2 is not satisfied for $T_{w,in,re}$ = 38ºC, case 4, as well as $T_{w,in,re}$ = 44ºC, case 1 and case 2. However, to validate that condition 2 is justified, simulations are still conducted for the aforementioned conditions and the results are graphically presented.

Table 4: Air-states, fluid flow and operating conditions under which the operation of an actual HMX is simulated

$U_{a,de}$	2 m/s	$T_{w,in,cold}$	30°C	Y_r	0.011 kg/kg d.a.
$U_{a,re}$	-2 m/s	$T_{w,in,hot}$	38, 44, 50°C	$T_{r,in}$	13 °C
$\dot{m}_{w,hot}$	5 kg/s	T_o	32°C	$Y_{r\ in}$	0.0094 kg/kg d.a
$\dot{m}_{w,cool}$	5 kg/s	Y_o	0.02 kg/kg d.a.		
t_1, t_2	180 s	T_r	25°C		

Table 5: Air-streams' conditions and evaluated intermediate variables based on steps for designing an HMX described in Table 1 and Figure 4 (notations V_{O1}, V_{R1}, V_{O2}, V_{R2} are consistent with those in Figure 1)

		Dehumidification air-stream				**Regeneration air-stream**				**Evaluated parameters based on "Steps for designing an HMX"**														
$T_{w,in,re}$	**Case No.**	**Fresh air proportion (V_{O1})**	**Room-return air proportion (V_{R1})**	**$T_{a,in,de}$**	**$Y_{a,in,de}$**	**Fresh air proportion (V_{O2})**	**Room-return air proportion (V_{R2})**	**$T_{a,in,re}$**	**$Y_{a,in,re}$**	**$Y_{a,o,de,min}$**	**Condition 1 satisfied?**	**$T_{w,de}$**	**$T_{w,re}$**	**λ**	**t_{tw}**	**$Y_{a,o,de-tw,avg}$**	**$Y_{a,o,de-cw,avg}$**	**$Y_{a,o,de,min-real}$**	**Condition 2 satisfied?**	**$Y_{a,o,re-avg}$**	**$W(\varphi_{final})$**	**$W(\varphi_{initial})$**	**L_x/P_f ($C_f = 1$)**	**L_x**
38	1	0	1	25	0.011	1	0	32	0.02	0.01263	N	-	-	-	-	-	-	-	-	-	-	-	-	1.008
38	2	0.25	0.75	26.75	0.01325	0.75	0.25	30.25	0.01775	0.01122	N	-	-	-	-	-	-	-	-	-	-	-	-	1.008
38	3	0.5	0.5	28.5	0.0155	0.5	0.5	28.5	0.0155	0.00981	N	-	-	-	-	-	-	-	-	-	-	-	-	1.008
38	4	0.75	0.25	30.25	0.01775	0.25	0.75	26.75	0.01325	0.00840	Y	30.8	36.8	0.049	50.6	0.01133	0.00865	0.00980	N	0.0216	0.29227	0.28192	945	1.008
38	5	1	0	32	0.02	0	1	25	0.011	0.00698	Y	31.1	36.5	0.072	33.4	0.01020	0.00922	0.00893	Y	0.0216	0.29540	0.26662	432	1.008
44	1	0	1	25	0.011	1	0	32	0.02	0.00913	Y	30.0	43.4	0.140	23.5	0.01470	0.00861	0.00941	N	0.0216	0.26072	0.25248	227	0.504
44	2	0.25	0.75	26.75	0.01325	0.75	0.25	30.25	0.01775	0.00812	Y	30.2	43.1	0.165	19.7	0.01358	0.00888	0.00889	N	0.0216	0.27576	0.24363	140	0.504
44	3	0.5	0.5	28.5	0.0155	0.5	0.5	28.5	0.0155	0.00710	Y	30.5	42.8	0.166	19.3	0.01245	0.00903	0.00836	Y	0.0216	0.28604	0.23369	137	0.504
44	4	0.75	0.25	30.25	0.01775	0.25	0.75	26.75	0.01325	0.00608	Y	30.8	42.6	0.165	19.1	0.01133	0.00917	0.00783	Y	0.0216	0.29227	0.22269	141	0.504
44	5	1	0	32	0.02	0	1	25	0.011	0.00506	Y	31.1	42.3	0.163	19.1	0.01020	0.00931	0.00730	Y	0.0216	0.29540	0.21073	147	0.504
50	1	0	1	25	0.011	1	0	32	0.02	0.00670	Y	30.0	49.2	0.466	7.8	0.01470	0.00916	0.00735	Y	0.0216	0.26072	0.19404	28	0.210
50	2	0.25	0.75	26.75	0.01325	0.75	0.25	30.25	0.01775	0.00596	Y	30.2	48.9	0.412	8.8	0.01358	0.00919	0.00706	Y	0.0216	0.27576	0.18652	51	0.210
50	3	0.5	0.5	28.5	0.0155	0.5	0.5	28.5	0.0155	0.00522	Y	30.5	48.6	0.381	9.4	0.01245	0.00923	0.00676	Y	0.0216	0.28604	0.17848	67	0.210
50	4	0.75	0.25	30.25	0.01775	0.25	0.75	26.75	0.01325	0.00447	Y	30.8	48.3	0.359	9.9	0.01133	0.00929	0.00646	Y	0.0216	0.29227	0.16996	80	0.210
50	5	1	0	32	0.02	0	1	25	0.011	0.00372	Y	31.1	48.1	0.340	10.4	0.01020	0.00935	0.00616	Y	0.0216	0.29540	0.16104	92	0.210

Figure 8 (a), (b) and (c) show the dehumidified air specific humidity and temperature versus C_f (and $1/P_f$) for $T_{w,in,re}$ = 38ºC, case 4, $T_{w,in,re}$ = 44ºC, case 1, and $T_{w,in,re}$ = 44ºC, case 2, respectively. In all three cases, irrespective of the value of C_f (and P_f), $Y_{a,o,de,avg}$ is larger than $Y_{r,in}$. For the case of Figure 8 (a), the designed HMX performs reasonably well by reducing the humidity from $Y_{a,in,de}$ = 0.01775 kg/kg dry air to $Y_{a,o,de,avg}$ of ≈0.0106 kg/kg dry air, however it does not satisfy the requirement of achieving a specific humidity of 0.0094 kg/kg dry air ($Y_{r,in}$). When C_f is varied from 1 to 1.2, $Y_{a,o,de,avg}$ slightly increases although the desiccant surface area increases. This is due to the increase in thermal mass with increase in C_f, which in turn increases the time-period of the thermal-wave during which the performance is relatively poor. This is also evident by observing the T versus C_f curve. Values of C_f larger than 1.2 were not tested for this case since (i) the trend of $Y_{a,o,de,avg}$ was anyways increasing with C_f and could not have approached $Y_{r,in}$, and (ii) the larger C_f, the smaller is the value of P_f ; for this case, P_f becomes smaller than the maximum value for which the correlation used to determine the heat transfer coefficient (and by extension, the mass transfer coefficient) is valid. For the case of Figure 8(b), C_f is varied from 1 to 1.9, the trend in $Y_{a,o,de,avg}$ is again slightly increasing, and the HMX is only able to reduce the specific humidity from 0.011 ($Y_{a,in,de}$) to 0.0104 kg/kg dry air. For the case of Figure 8(c), as C_f is varied from 1 to 1.6, $Y_{a,o,de,avg}$ decreases from 0.0102 to 0.0098 kg/kg dry air, but remains flat at 0.0098 kg/kg when C_f is further increased from 1.6 to 1.9. *Thus, condition 2 correctly anticipates the conditions under which an HMX would not be able to meet the specific humidity requirement of the dehumidified air-stream.*

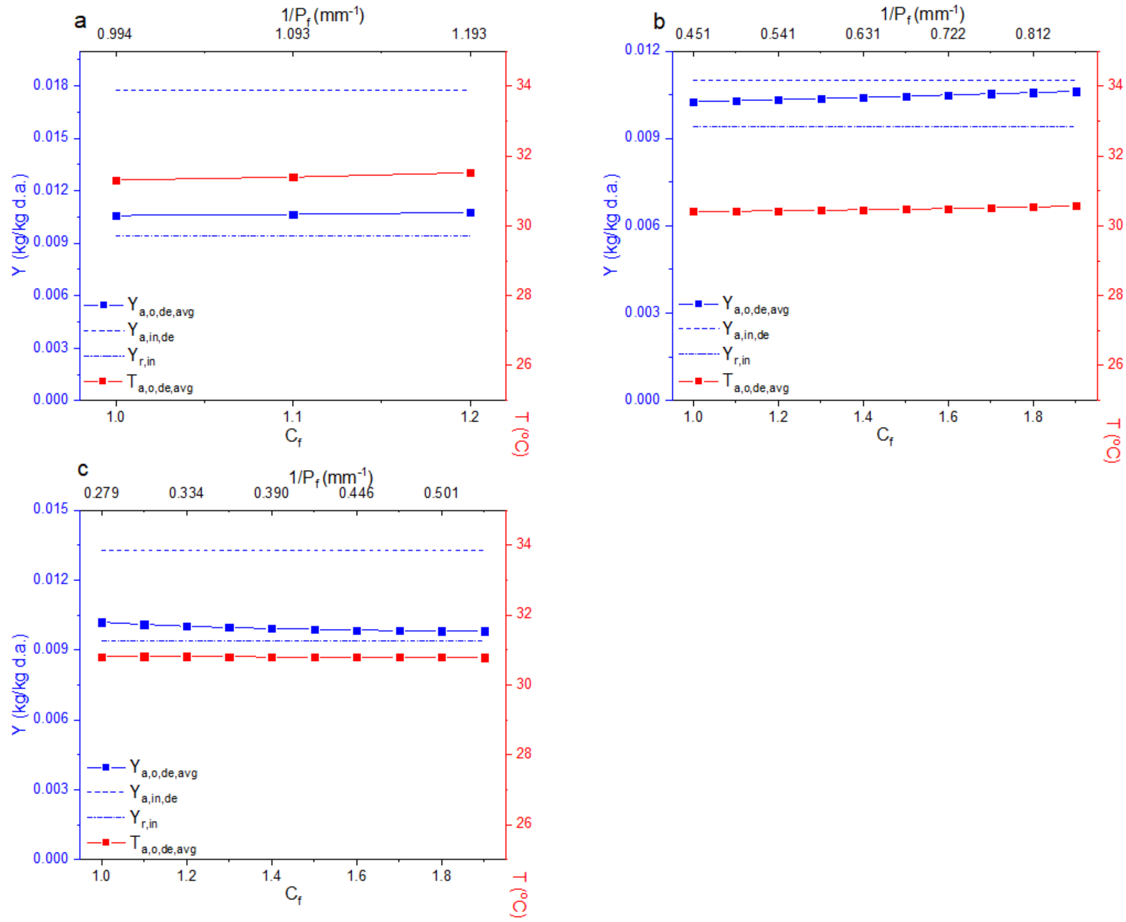

Figure 8: Dehumidified air specific humidity (blue) and temperature (red) versus C_f (and $1/P_f$) for (a) $T_{w,in,re}$ = 38ºC, case 4, (b) $T_{w,in,re}$ = 44ºC, case 1, and (c) $T_{w,in,re}$ = 44 ºC, case 2.

Figure 9(a) and (b) respectively show the transient variations in outlet specific humidity and temperature for $T_{w,in,re}$ = 38ºC, case 5. In Figure 9(a), $Y_{a,o}$ is plotted for value of C_f = 1 as well as 1.3. Over and above the outlet specific humidity, Figure 9(a) also shows the inlet specific humidity ($Y_{a,in}$) and the target outlet specific humidity during dehumidification ($Y_{r,in}$) as well as the minimum possible outlet specific humidity ($Y_{a,o,de,min}$) realized in case of an ideal HMX. Notice also that the time-period of the prevalence of the thermal wave (t_{tw}) and the average specific humidity during thermal-wave of the dehumidification process ($Y_{a,o,de\text{-}tw,avg}$) as evaluated using the method described in Section 4 and as summarized in Table 5 is also shown on the graphs. The dotted oblique line segment from $t = 0$ to t_{tw} is the simplified linear trend assumed (equation (64)) in $Y_{a,o,de}$ during the thermal wave. The bold dot indicated by the arrow-head is $Y_{a,o,de\text{-}tw,avg}$ as evaluated by equation (64); from visual inspection, it can be concluded that the evaluated $Y_{a,o,de\text{-}tw,avg}$ is reasonably close to the simulation average value inferred from the transient trend in $Y_{a,o}$ from $t = 0$ to t_{tw}. As shown in Figure 9(b), t_{tw} evaluated using equation (72) well predicts the time required for cooling down of the air-stream to within 0.5ºC of the quasi-steady value during the concentration wave. It may also be noted that during the concentration wave, $T_{a,o}$ approaches T_{ref}, evaluated using the method described in Section 4.

From Figure 9(a), it can be observed that the outlet specific humidity during the thermal wave is higher than that during the concentration wave. During dehumidification, as time progresses, the $Y_{a,o}$ decreases with decreasing $T_{a,o}$, $Y_{a,o}$ reaches a minimum and then increases gradually with a small slope. The minimum is smaller for the case of C_f = 1.3 than it is for C_f = 1 since for the former a greater quantity of desiccant is available, which is better able to dehumidify air before it starts becoming saturated enough for the $Y_{a,o}$ to start increasing. As the process switches from dehumidification to regeneration at t = 180 s, $Y_{a,o}$ quickly increases along with $T_{a,o}$, reaches a maximum and then decreases gradually. Just as during dehumidification, during regeneration $Y_{a,o}$ is lower for C_f = 1.3 compared to C_f = 1, and $Y_{a,o}$ is larger for the case of C_f =1.3 compared to that of C_f = 1, since the larger the amount of moisture adsorbed by the desiccant during dehumidification, the larger will be the amount of moisture released during regeneration. Notice that $Y_{a,o,de,min}$ (0.007 kg/kg d.a.) is significantly lower than the $Y_{a,o}$ realized for both cases. The outlet temperature $T_{a,o}$ curves for both values of C_f are very close to each other.

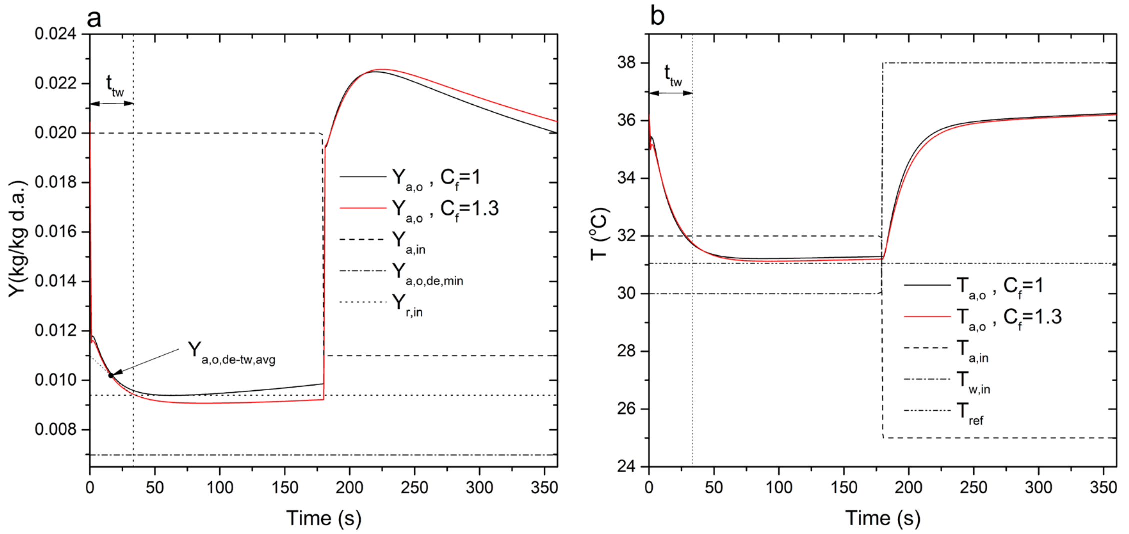

Figure 9: Transient specific humidity (a) and temperature (b) of the output air stream for $T_{w,in,re}$ = 38ºC, case 5.

It is evident from Figure 9 that some of the intermediate variables evaluated using the methodology described in Section 4, namely, t_{tw}, T_{ref} (or $T_{w,de}$) and $Y_{a,o,de\text{-}tw,avg}$ are in good agreement with the corresponding values of the simulation results. Except for the period of the thermal-wave, the specific humidity $Y_{a,o}$ of the outlet air during dehumidification is very close to $Y_{r,in}$ (the target value) even for C_f = 1. These observations serve to justify (although approximate) the design methodology described in Section 4.

Figure 10(a) shows that the average outlet air specific humidity $Y_{a,o,de,avg}$ decreases with increase in C_f (and $1/P_f$), or conversely that moisture removed ($Y_{a,in}$ - $Y_{a,o,de,avg}$) increases with decreasing fin pitch P_f, since the smaller the P_f, the greater the number of fins, implying a larger mass of desiccant available for dehumidification and a larger mass transfer surface area. Note that when C_f is low, $Y_{a,o,de,avg}$ is slightly larger than $Y_{r,in}$; this is because equation (50) used to determine the dimensions of the HMX uses values of $W(\phi_{final})$ and $W(\phi_{initial})$ derived assuming negligible mass-transfer resistance, which results in a slight under-estimation of the value of $1/P_f$ required to realize the targeted specific humidity $Y_{r,in}$. The average outlet air specific humidity during dehumidification $Y_{a,o,de,avg}$ meets the target value $Y_{r,in}$ for C_f = 1.3 and $T_{a,o,de,avg}$ remains nearly constant because the adsorption heat released is nearly the same for all C_f values tested. This is because the moisture removal ($Y_{a,in,de}$ $-Y_{a,o,de,avg}$) is nearly the same for all cases. As the dehumidification performance becomes better with decreasing P_f (increasing C_f), the effectiveness (ε_{RH} and ε_Y) values improve. The effectiveness values range between approximately 0.8 and 0.9 with ε_{RH} being consistently larger than ε_Y. The considered design of the HMX thus results in an efficient dehumidification performance. The coefficient of performance, total cooling load CL_{total} (handled by the complete hybrid system), the cooling load CL_{HMX} handled by the HMX, as well as the extra fluid power FP required for retrofitting an HMX to a conventional system (to yield the hybrid system schematically shown in Figure 1) is plotted against C_f (and $1/P_f$) in Figure 10(b). The coefficient of performance as well as CL_{HMX} improve with increasing C_f (decreasing P_f) and the required fluid power (FP) increases as well. For C_f = 1.3, since CL_{HMX} is 6.6 times the fluid power required and the cooling coefficient of performance is approximately 10 (significantly larger than the base-line $COP_{conventional}$ of 4), the HMX is well suited for this case. Notice that CL_{HMX} = 45.6 kW while total cooling load CL (on hybrid air-conditioning system) = 77 kW; the HMX thus handles 60% of the total cooling load.

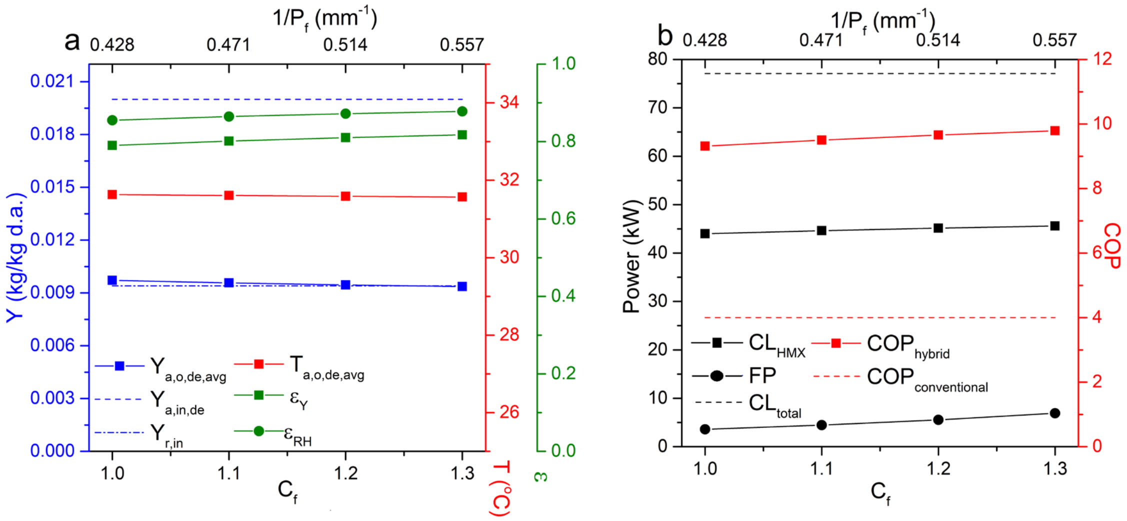

Figure 10: Performance characteristics for a hot water inlet temperature of $T_{w,in,re}$ = 38ºC, case 5. (a) average outlet air specific humidity (blue), temperature (red) and efficiency coefficients ε_Y and ε_{RH} (green) versus C_f (and $1/P_f$); (b) total and HMX cooling load and fluid power (black) and coefficient of performance of the conventional and hybrid system (red) versus C_f (and $1/P_f$).

Graphical results for $T_{w,in,re}$ = 44ºC and 50ºC are not shown in the paper to avoid showing results that are qualitatively similar to those shown in Figure 9 and Figure 10. For the sake of completeness however, the results are included in the Supplementary material (Figures 6,7 and 8). Table 6 summarizes the results pertaining to Figure 10 and Supplementary material's Figures 6,7 and 8 for C_f = 1 and the value of C_f for which $Y_{a,o,de,avg}$ equals the target value $Y_{r,in}$.

Table 6: Summary of results for a ICHDHMX retrofitted to a conventional HVAC system with a cooling COP of 4.

$T_{w,in,re}$	Case	C_f	P_f	$Y_{a,in,de}$	$Y_{a,o,de,avg}$	$Y_{a,o,de,min}$	$T_{a,in,de}$	$T_{a,o,de,avg}$	ε_Y	ε_{RH}	CL_{HMX}	FP	CL_{total}	COP_{new}
38	5	1	2.34	0.02	0.0097	0.0070	32	31.6	0.79	0.86	43.98	3.60	77.1	9.32
		1.3	1.80		0.0094			31.6	0.82	0.88	45.58	6.90		9.79
44	3	1	3.69	0.0155	0.0102	0.0071	28.5	31.3	0.63	0.71	17.70	0.84	52.3	6.05
		1.7	2.17		0.0094			31.2	0.73	0.80	21.46	2.14		6.78
	4	1	3.58	0.01775	0.0102	0.0061	30.25	31.8	0.65	0.73	29.55	0.87	64.6	7.37
		1.3	2.75		0.0094			31.7	0.71	0.79	32.78	1.32		8.11
	5	1	3.44	0.02	0.0100	0.0051	32	32.3	0.67	0.75	41.62	0.92	77.1	8.69
		1.2	2.86		0.0093			32.2	0.72	0.79	44.67	1.23		9.51
50	1	1	8.04	0.011	0.0101	0.0067	25	28.4	0.22	-0.02	-1.84	0.20	27.7	3.75
		1.9	4.23		0.0094			29.7	0.37	0.33	-1.30	0.30		3.82
	2	1	4.15	0.01325	0.0104	0.0060	26.75	30.5	0.40	0.43	5.92	0.31	40	4.69
		1.6	2.59		0.0093			31.0	0.54	0.61	9.39	0.62		5.23
	3	1	3.16	0.0155	0.0105	0.0052	28.5	31.5	0.49	0.57	16.11	0.45	52.3	5.78
		1.4	2.26		0.0094			31.7	0.59	0.67	20.32	0.83		6.54
	4	1	2.63	0.01775	0.0105	0.0045	30.25	32.3	0.55	0.64	27.31	0.61	64.6	6.93
		1.3	2.02		0.0094			32.4	0.63	0.72	31.74	1.08		7.86
	5	1	2.27	0.02	0.0103	0.0037	32	33.0	0.59	0.69	39.07	0.82	77.1	8.14
		1.2	1.89		0.0094			33.0	0.65	0.74	42.88	1.28		9.05

It may be observed from Table 6 that for $T_{w,in,re}$ = 44 ºC case 3, wherein $Y_{a,in,de}$ is low (and simultaneously $Y_{a,in,re}$ is high), the C_f value at which $Y_{a,o,de,avg}$ approaches $Y_{r,in}$ is relatively higher while as $Y_{a,in,de}$ increases (and simultaneously $Y_{a,in,re}$ reduces), C_f value at which $Y_{a,o,de,avg}$ approaches $Y_{r,in}$ decreases (1.3 and 1.2 for cases 4 and 5 respectively). Notice that as the proportion of fresh-air increases from case 3 to 5 (See Table 5), $T_{a,in,de}$ and $Y_{a,in,de}$ increase and so does the total cooling load CL_{total} and CL_{HMX}. Thus, while retrofitting the HMX offers considerable advantage for all the three cases (notice that the COP is substantially improved and FP is negligible compared to CL_{HMX}), the greatest improvement in COP is realized for case 5 for which inlet humidity (and of course the latent heat load) is maximum.

Note from Table 5 that for cases pertaining to $T_{w,in,re}$ = 50 ºC, L_x = 0.21 m, which is much smaller compared to L_x for lower $T_{w,in,re}$. Therefore, the effectiveness (ε_{RH} and ε_Y) values are relatively lower since the surface area is smaller owing to smaller L_x and relatively larger P_f. It may be noted that the fin pitch is highest for case 1 and lowest for case 5, therefore the heat and mass transfer coefficients as well as the surface area are lowest for case 1 resulting in lower effectiveness values of the former. Notice that $\varepsilon_{RH} \approx 0$ for $C_f = 1$ for case 1. This is because, although the amount of moisture removed from the air is non-zero (resulting in a non-zero value of ε_Y), the low air temperature $T_{a,o,de,avg}$ caused the relative humidity at the outlet to be close to that at the inlet. For cases 2 to 5, it is easily noticeable that the coefficient of performance of the hybrid system is improved compared to that of the conventional system. Also, the extra fluid power required is much smaller compared to the cooling load handled by the HMX. Thus, use of an HMX is well justified for these cases. For case 1 however, it is clear that the cooling load handled by HMX is negative. This is because for this case, 100% of the room-return air is being handled by the HMX. Room air has a small latent heat load, since ($Y_r - Y_{r,in}$) is 0.0016 kg/kg dry air, but a substantial sensible heat load. Although the HMX manages all the latent heat load, it increases the temperature of the room-return air from 25ºC to nearly 30 ºC. This means that the use of an HMX adds sensible load to the air to be treated resulting in net enthalpy-gain of air. Therefore, the HMX should not be used under inlet conditions of case 1.

Taking a holistic view of Figure 10 and Table 6 (or Figures 6, 7 and 8 in the Supplementary material), the design methodology, even without the knowledge of C_f (i.e. when its value is assumed to be 1), provides an excellent starting point to conduct a parametric study to determine the critical geometrical parameters of the HMX that would help achieve the targeted dehumidification performance. It is worth noting that even if corrections are not made to account for the difference between idealized and real sorbate uptake (meaning that if $C_f = 1$), the outlet humidity for all tested cases was within 0.0011 kg/kg dry air of the targeted value of $Y_{r,in}$ (9.4 g/kg dry air). Thus, the design methodology works reasonably well. However, knowledge (or an educated guess) regarding the value of C_f would certainly be helpful in achieving the outlet specific humidity of the dehumidified air more precisely at the targeted value. The optimal value of C_f is found to be ranging from 1.2 to 1.9. For cases with smaller $Y_{a,in,de}$ but large $Y_{a,in,re}$, the value of C_f is on the higher side, while for cases with larger $Y_{a,in,de}$ but small $Y_{a,in,re}$, the value of C_f is on the lower side in this range.

6. Conclusions

In this work, low-grade heat driven, internally cooled and heated desiccant-coated heat and mass exchangers (ICHDHMX) are studied using an experimentally validated comprehensive heat and mass transfer model. Important contributions and findings of this work are as follows:

- The concept of an ideal HMX was specified and expressions for the performance of such an ideal exchanger were derived and validated.
- A simple graphical (psychrometric-chart based) methodology was presented as an alternative to determine the ideal (limiting) performance of the HMX.
- The humidity-ratio effectiveness (ε_Y) and relative-humidity effectiveness (ε_{RH}) for ICHDHMX were defined such that for a close-to-ideal HMX, their values approach 1. This was validated as well.
- A simple, non-iterative methodology was presented (avoiding complicated numerical modelling), which helps to determine whether an HMX is feasible, under the given inlet conditions of air and water-streams, and helps to estimate the geometric dimensions of the HMX in a straight-forward manner without the need for arduous comprehensive modeling and simulation.
- Using the comprehensive model, several cases were simulated for a range of inlet air-stream conditions, keeping the cooling water temperature constant at 30°C. All cases pertained to 250 µm thick silica-gel coating on both the sides of the fins of the HMX. Simulation results indicate that the design methodology, without the use of any tuning or correction factor ($C_f = 1$), can help design an HMX that could yield an outlet humidity of dehumidified air to within 0.0011 kg/kg dry air of the targeted value of $Y_{r,in}$ (9.4 g/kg dry air). For cases requiring precise outlet specific-humidity conditions, only a single tuning parameter C_f is required to improve the geometric design of the HMX. The value of C_f ranges between 1.2 and 1.9 for the cases presented here.
- When hot water at 50°C is available for regeneration, an HMX is feasible for all cases. For cases 2 to 5, the performance of HMX is excellent, delivering a cooling COP of up to nearly 10 (where the conventional COP was 4) while requiring relatively very low extra fluid power. Effectiveness values of up to 0.88 were observed with ε_{RH}

generally being larger than ε_Y. The larger the depth (L_x) and smaller the fin pitch (P_f) of the HMX, the larger was its effectiveness.

7. Recommendations for future work

- A noteworthy observation from Figure 10 as well as Figures 6, 7 and 8 in the Supplementary material is that the effectiveness values (ε_{RH} and ε_Y) are nearly independent of the inlet conditions of the air-streams, given a specific design of HMX (L_x, P_f, etc). Table 7 concisely illustrates that, given a particular value of L_x and approximate value of P_f clubbed under the same 'Sr. No' column in Table 7, ε_Y is nearly the same, and so is ε_{RH}. This is characteristic of the definition of heat-transfer effectiveness ε_T of heat exchangers: given a specific geometrical design of a heat exchanger and flow-configuration, equations and charts exist which help evaluate ε_T (see Incropera and Dewitt [43]). The fact that the value of ε_T is independent of the inlet conditions of the heat exchanging fluids and that ε_T can be evaluated based on the knowledge of the Number of Transfer Units is something that makes evaluation of the heat exchanger performance relatively easy instead of having to use detailed and cumbersome simulation models. An analogous observation regarding mass-exchanging fluids (air-streams) hints at the possibility that it may be possible to derive expressions for mass-transfer effectiveness (ε_{RH} and ε_Y). This, however, is beyond the scope of the present work and is recommend as a plausible direction for future investigation.

Table 7: Observed similarities in the values of ε_Y and ε_{RH} for the same HMX design but different inlet air-stream conditions

$T_{w,in,re}$	Sr. No.	Case No.	L_x (m)	P_f (mm) range	ε_Y range	ε_{RH} range
44	1	3	0.504	3.69-2.63	0.63-0.7	0.71-0.78
		4		3.58-2.75	0.65-0.71	0.73-0.79
		5		3.44-2.86	0.67-0.72	0.75-0.79
50	2	2	0.210	3.19-2.59	0.48-0.54	0.54-0.61
		3		3.16-2.63	0.49-0.54	0.57-0.63
	3	3		2.63-2.26	0.54-0.59	0.63-0.67
		4		2.63-2.19	0.55-0.60	0.64-0.69
	4	4		2.19-2.02	0.60-0.63	0.69-0.72
		5		2.27-2.06	0.59-0.62	0.69-0.71

- While it is true that silica gel is among the most commonly used desiccant and its coating thickness typically ranges from 100-250 µm, it is quite possible that another desiccant with substantially lower moisture diffusivity and/or a thicker coating may be used. In such cases, C_f is expected to be larger than the values determined in this study. It is therefore pertinent to carry out a similar study for various desiccants (especially those with significantly lower moisture diffusivity) and with a thicker coating.
- The focus of this work was on dehumidification exclusively by adsorption phenomena (not condensation). There may be cases wherein cool water flowing through the tubes is below the dew-point temperature of the air-stream to be dehumidified. Such cases require consideration of a combination of condensation over and above the adsorption phenomena. This is a potential direction for future work.
- Practically, it is quite plausible that instead of hot water, it is hot air that is available, for instance in case of an air-conditioning unit having an air-cooled (not water-cooled) condenser. Therefore, cases where quasi-isothermal dehumidification (same process as studied here) and isenthalpic regeneration (process similar to that occurring in the regeneration section of the desiccant wheel) occur, are also significant. Such cases shall be studied in our future work.

Acknowledgement

The authors gratefully acknowledge the research funding received from the National Research Foundation (NRF). This was under EIRP (Energy Innovation Research Programme) R-263-000-B82-279, managed on behalf of BCA (Building and Construction Authority).

References

[1] Pérez-Lombard L, Ortiz J, Pout C. A review on buildings energy consumption information. Energy Build 2008;40:394–8. doi:10.1016/j.enbuild.2007.03.007.

[2] Goetzler W, Zogg R, Young J, Johnson C. Energy savings potential and RD&D opportunities for non-vapor-compression HVAC technologies. 2014.

[3] Pennington NA. Humidity changer for air-conditioning. 2,700,537, 1955.

[4] Tu R, Liu XH, Jiang Y. Performance analysis of a two-stage desiccant cooling system. Appl Energy 2014;113:1562–74. doi:10.1016/j.apenergy.2013.09.016.

[5] Pandelidis D, Anisimov S, Worek WM, Drag P. Comparison of desiccant air conditioning systems with different indirect evaporative air coolers. Energy Convers Manag 2016;117:375–92. doi:10.1016/j.enconman.2016.02.085.

[6] Tu YD, Wang RZ, Ge TS, Zheng X. Comfortable , high-efficiency heat pump with desiccant-coated , water-sorbing heat exchangers. Sci Rep 2017:1–10. doi:10.1038/srep40437.

[7] Oh SJ, Ng KC, Thu K, Kum Ja M, Islam MR, Chun W, et al. Studying the performance of a dehumidifier with adsorbent coated heat exchangers for tropical climate operations. Sci Technol Built Environ 2017;23:127-135. doi:10.1016/j.energy.2017.02.169.

[8] Ren CQ, Tu M, Wang HH. An analytical model for heat and mass transfer processes in internally cooled or heated liquid desiccant-air contact units. Int J Heat Mass Transf 2007;50:3545–55. doi:10.1016/j.ijheatmasstransfer.2006.12.034.

[9] Kumar A, Yadav A. Experimental investigation of solar driven desiccant air conditioning system based on silica gel coated heat exchanger. Int J Refrig 2016;69:51–63. doi:10.1016/j.ijrefrig.2016.05.008.

[10] Zhao Y, Dai YJ, Ge TS, Wang HH, Wang RZ. A high performance desiccant dehumidification unit using solid desiccant coated heat exchanger with heat recovery. Energy Build 2016;116:583–92. doi:10.1016/j.enbuild.2016.01.021.

[11] Vivekh P, Bui DT, Wong Y, Kumja M, Chua KJ. Performance evaluation of PVA-LiCl coated heat exchangers for next-generation of energy-efficient dehumidification. Appl Energy 2019;237:733–50. doi:10.1016/j.apenergy.2019.01.018.

[12] Vivekh P, Bui DT, Kumja M, Islam MR, Chua KJ. Theoretical performance analysis of silica gel and composite polymer desiccant coated heat exchangers based on a CFD approach. Energy Convers Manag 2019;187:423–46. doi:10.1016/j.enconman.2019.02.093.

[13] Cui X, Liu Y, Liu Y, Jin L, Zhao M, Meng X. Studying the performance of a liquid desiccant indirect evaporative cooling system. Energy Procedia 2019;158:5659–65. doi:10.1016/j.egypro.2019.01.571.

[14] Jagirdar M, Pandelidis D, Pacak A, Worek W, Cetin S. Performance evaluation of an air conditioning system based on quasi isothermal dehumidifcation. Energy Convers Manag 2020;217:113009. doi:10.1016/j.enconman.2020.113009.

[15] Hu LM, Ge TS, Jiang Y, Wang RZ. Performance study on composite desiccant material coated fin-tube heat exchangers. Int J Heat Mass Transf 2015;90:109–20. doi:http://dx.doi.org/10.1016/j.ijheatmasstransfer.2015.06.033.

[16] Worek WM, Chung-Ju M. Simulation of an integrated hybrid desiccant vapor-compression cooling system. Energy 1986;11:1005–21. doi:10.1016/0360-5442(86)90031-9.

[17] Li Z, Michiyuki S, Takeshi F. Experimental study on heat and mass transfer characteristics for a desiccant-coated fin-tube heat exchanger. Int J Heat Mass Transf 2015;89:641–51. doi:10.1016/j.ijheatmasstransfer.2015.05.095.

[18] Jagirdar M, Lee PS. Mathematical modeling and performance evaluation of a desiccant coated fin-tube heat exchanger. Appl Energy 2018;212:401–15. doi:10.1016/j.apenergy.2017.12.038.

[19] Zhou X, Goldsworthy M, Sproul A. Performance investigation of an internally cooled desiccant wheel. Appl Energy 2018;224:382–97. doi:10.1016/j.apenergy.2018.05.011.

[20] Erkek TU, Gungor A, Fugmann H, Morgenstern A, Bongs C. Performance evaluation of a desiccant coated heat exchanger with two different desiccant materials. Appl Therm Eng 2018;143:701–10. doi:10.1016/j.applthermaleng.2018.06.012.

[21] Yonggao Y, Xiaosong Z, Geng W, Lei L. Experimental study on a new internally cooled/heated dehumidifier/regenerator of liquid desiccant systems. Int J Refrig 2008;31:857–66. doi:10.1016/j.ijrefrig.2007.10.004.

[22] Yin Y, Zhang X, Peng D, Li X. Model validation and case study on internally cooled/heated dehumidifier/regenerator of liquid desiccant systems. Int J Therm Sci 2009;48:1664–71. doi:10.1016/j.ijthermalsci.2008.12.017.

[23] Vivekh P, Kumja M, Bui DT, Chua KJ. Recent developments in solid desiccant coated heat exchangers – A review. Appl Energy 2018;229:778–803. doi:10.1016/j.apenergy.2018.08.041.

[24] Oh SJ, Ng KC, Chun W, Chua KJE. Evaluation of a dehumidifier with adsorbent coated heat exchangers for

tropical climate operations. Energy 2017;137:441–8. doi:10.1016/j.energy.2017.02.169.
[25] Narayanan R, Saman WY, White SD. A non-adiabatic desiccant wheel: Modeling and experimental validation. Appl Therm Eng 2013;61:178–85. doi:10.1016/j.applthermaleng.2013.07.007.
[26] Sun XY, Dai YJ, Ge TS, Zhao Y, Wang RZ. Heat and mass transfer comparisons of desiccant coated microchannel and fin-and-tube heat exchangers. Appl Therm Eng 2019;150:1159–67. doi:10.1016/j.applthermaleng.2019.01.071.
[27] Jagirdar M, Ong WL, Ho GW, Lee PS. Experimental investigations on desiccant coated fin tube heat exchangers retrofitted to a conventional HVAC system. Int. Conf. Appl. Energy 2019, 2019.
[28] Ge TS, Li Y, Wang RZ, Dai YJ. A review of the mathematical models for predicting rotary desiccant wheel. Renew Sustain Energy Rev 2008;12:1485–528. doi:10.1016/j.rser.2007.01.012.
[29] Ge TS, Dai YJ, Wang RZ. Performance study of silica gel coated fin-tube heat exchanger cooling system based on a developed mathematical model. Energy Convers Manag 2011;52:2329–38. doi:10.1016/j.enconman.2010.12.047.
[30] Jeong J, Yamaguchi S, Saito K, Kawai S. Performance analysis of desiccant dehumidification systems driven by low-grade heat source. Int J Refrig 2011;34:928–45. doi:10.1016/j.ijrefrig.2010.10.001.
[31] Hua LJ, Ge TS, Wang RZ. Extremely high efficient heat pump with desiccant coated evaporator and condenser. Energy 2019;170:569–79. doi:10.1016/j.energy.2018.12.169.
[32] Sphaier LA, Worek WM. Parametric analysis of heat and mass transfer regenerators using a generalized effectiveness-NTU method. Int J Heat Mass Transf 2009;52:2265–72. doi:10.1016/j.ijheatmasstransfer.2008.11.017.
[33] Nobrega CEL, Brum NCL. Desiccant assisted cooling: fundamentals and applications. 2014.
[34] Goldsworthy M, White SD. Limiting performance mechanisms in desiccant wheel dehumidification. Appl Therm Eng 2012;44:21–8. doi:10.1016/j.applthermaleng.2012.03.046.
[35] Ali Mandegari M, Pahlavanzadeh H. Introduction of a new definition for effectiveness of desiccant wheels. Energy 2009;34:797–803. doi:10.1016/j.energy.2009.03.001.
[36] Nóbrega CEL, Brum NCL. A graphical procedure for desiccant cooling cycle design. Energy 2011;36:1564–70. doi:10.1016/j.energy.2011.01.002.
[37] Abe OO, Simonson CJ, Besant RW, Shang W. Effectiveness of energy wheels from transient measurements Part I: Prediction of effectiveness and uncertainty. Int J Heat Mass Transf 2006;49:52–62. doi:10.1016/j.ijheatmasstransfer.2005.08.009.
[38] Van den Bulck E, Mitchell JW, Klein S a. Design theory for rotary heat and mass exchangers — II. Effectiveness-number-of-transfer-units method for rotary heat and mass exchangers. Heat Mass Transf 1985;28:1587–95.
[39] Collier RK. Desiccant Dehumidification and Cooling Systems Assessment and Analysis 1997;99352.
[40] Shah RK, Sekulic. DP. Fundamentals of heat exchanger design. John Wiley & Sons; 2003.
[41] Cui X, Mohan B, Islam MR, Chou SK, Chua KJ. Energy performance evaluation and application of an air treatment system for conditioning building spaces in tropics. Appl Energy 2017;204:1500–12. doi:https://doi.org/10.1016/j.apenergy.2017.03.067.
[42] Zhang LZ, Zhu DS, Deng XH, Hua B. Thermodynamic modeling of a novel air dehumidification system. Energy Build 2005;37:279–86. doi:10.1016/j.enbuild.2004.06.019.
[43] Incropera, F. P., Dewitt DP. Fundamentals of heat and mass transfer. John Wiley & Sons; 2011.
[44] Ruivo CR, Costa JJ, Figueiredo AR, Kodama A. Effectiveness parameters for the prediction of the global performance of desiccant wheels - An assessment based on experimental data. Renew Energy 2012;38:181–7. doi:10.1016/j.renene.2011.07.023.
[45] Li Z, Liu XH, Lun Z, Jiang Y. Analysis on the ideal energy efficiency of dehumidification process from buildings. Energy Build 2010;42:2014–20. doi:10.1016/j.enbuild.2010.06.008.
[46] Kodama A, Hirayama T, Goto M, Hirose T, Critoph RE. The use of psychrometric charts for the optimisation of a thermal swing desiccant wheel. Appl Therm Eng 2001;21:1657–74. doi:10.1016/S1359-4311(01)00032-1.
[47] Mei VC, Chen FC, Lavan Z, Collier Jr RK, Meckler G. An Assessment of Desiccant and Cooling Dehumidification Technology. Oak Ridge: 1992.